Journal of Volcanology and Geothermal Research 454 (2024) 108160

Contents lists available at ScienceDirect

Journal of Volcanology and Geothermal Research

journal homepage: www.journals.elsevier.com/journal-of-volcanology-and-geothermal-research

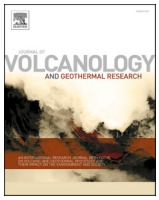

The 2019 pumice raft forming eruption of Volcano-F (Volcano 0403–091) and implications for hazards posed by submerged calderas

Isobel A. Yeo [a,*], Iona M. McIntosh [b], Scott E. Bryan [c], Kenichiro Tani [d], Matthew Dunbabin [e], Katherine J. Dobson [f], Samuel J. Mitchell [g], Patrick C. Collins [h], Michael A. Clare [a], Henrietta Cathey [c], Isikeli Duwai [i], Philipp A. Brandl [j], Karen Stone [k], Mele S. Manu [l]

[a] National Oceanography Centre Southampton, European Way, Southampton SO14 3ZH, UK
[b] Japan Agency for Marine-Earth Science and Technology (JAMSTEC), 2-15 Natsushima-cho, Yokosuka, Kanagawa 237-0061, Japan
[c] School of Earth & Atmospheric Sciences, Queensland University of Technology, 2 George St, Brisbane City, QLD 4000, Australia
[d] National Museum of Nature and Science, 7-20 Uenokoen, Taito City, Tokyo 110-8718, Japan
[e] School of Electrical Engineering & Robotics, Queensland University of Technology, 2 George St, Brisbane City, QLD 4000, Australia
[f] Department of Civil & Environmental Engineering, University of Strathclyde, 75 Montrose Street, Glasgow G1 1XJ, UK
[g] University of Bristol, Wills Memorial Building, Bristol BS8 1RL, UK
[h] Queen's University Belfast, University Rd, Belfast BT7 1NN, UK
[i] Department of Mineral Resources, Ministry of Lands and Mineral Resources, PO Box 2222, Government Building, Suva, Fiji
[j] GEOMAR Helmholtz Centre for Ocean Research Kiel, Wischhofstraße 1-3, 24148 Kiel, Germany
[k] Vava'u Environmental Protection Association (VEPA), Tonga
[l] Natural Resources Division, Ministry of Lands and Natural Resources, Tonga

ARTICLE INFO

Keywords:
Submarine volcanism
Pumice raft
Seafloor mapping
Explosive volcanism
Caldera

ABSTRACT

Low volcanic explosivity index (VEI) eruptions are common occurrences in the Southwest Pacific but, as demonstrated by the 2021/2022 eruption of Hunga Volcano, submerged calderas in the region are also capable of producing much larger and more hazardous eruptions. As such, characterising smaller events from potentially hazardous systems is essential. The 2019 eruption of Volcano-F, a submerged caldera, would likely have gone totally undetected had it not produced a pumice raft that inundated beaches in Fiji and eventually washed up in Australia. New data, acquired 5 months after the eruption, reveal the development of a new vent and the accumulation of at least $3.1*10^7$ m^3 bulk volume (dense rock equivalent of $5.6*10^6$ m^3) of material on the seafloor. Between 30 and 70% of erupted material entered the raft, while the rest remained near to or was dispersed down-current of the vent. This previously unaccounted for material increases the volume estimate for the eruption, confirming it as a VEI 3 event and highlights the importance of considering not just the floating component of a pumice raft forming eruption for VEI estimation. Geochemical analysis reveals the eruption comprised a homogenous batch of dacitic magma, with compositional characteristics similar to that erupted from the same volcano in 2001, and an until-now-unidentified pumice raft in the Coral Sea in 1964. Volcano-F therefore appears to have had at least three explosive eruptions in the last 60 years, indicating it is significantly at unrest. Repeated eruptions of similar composition and low crystal content magma over decadal to centennial scales indicate the existence of a melt-dominant magma body beneath the volcano. Submerged calderas, like Volcano-F, are common in the wider Southwest Pacific region, with many such calderas producing regular eruptions, implicating active magmatic recharge. Our findings motivate a need to carefully monitor and characterise even apparently small eruptions at this volcano, and others along the Tonga-Kermadec Arc. This is because such eruptions have the potential to subsequently prime or trigger more explosive eruptions and provide critical geochemical evidence about the plumbing system and evolution of the volcano, essential for understanding the diverse hazards they pose.

* Corresponding author.
E-mail address: i.yeo@noc.ac.uk (I.A. Yeo).

https://doi.org/10.1016/j.jvolgeores.2024.108160
Received 17 June 2024; Received in revised form 25 July 2024; Accepted 1 August 2024
Available online 3 August 2024

1. Introduction

1.1. Volcanoes of the Tofua Arc

The northern end of the Tonga-Kermadec Arc is one of the most volcanically active island arc regions on the planet. Volcanic records are incomplete because most volcanoes in the region are fully or partially submerged, remote from population centres and shipping routes, and have poor seismic and hydroacoustic monitoring, meaning many eruptions go undetected. The volcanoes of the Tofua Arc are highly variable. Their magma chemistries include basaltic andesites, andesites and dacites (Ewart et al., 1998), and their edifice morphologies range from monogenetic and composite cones to calderas, the seafloor relief of which is often characterised by large bedforms that radiate away from them (Pope et al., 2018). Of the 14 eruptions recorded so far this century, all but two had a Volcanic Explosivity Index (VEI) of 2 (Newhall and Self, 1982) or lower, and only six in the full Global Volcanism Program database of recorded eruptions had VEI >3 (Global Volcanism Program, 2024). While this is partly due to the limited characterisation of these eruptions and inaccuracies in their assigned VEIs, it is probable that most eruptions occurring along the Tofua Arc are VEI 3 or lower. Small and moderate volcanic eruptions can produce significant disruption from: i) ash and steam clouds that cause flight rerouting and cancellation; ii) navigational hazards created by changes in seafloor topography; iii) ash fall onto nearby regions; and iv) pumice rafts, which can float for months and pose a risk to vessels and coastal infrastructure. Moreover, eruptions of any size have the potential to cause flank failures that can generate devastating tsunamis. Importantly, although most recorded eruptions are < VEI 3, Tofua Arc volcanoes are capable of producing significant explosive eruptions. Their ocean setting produces a range of hazards to coastal communities and to subsea infrastructure, as demonstrated by the climactic VEI 5 eruption of Hunga Volcano (formerly Hunga Tonga – Hunga Ha'apai) in January 2022; the most explosive volcanic eruption this century (Borrero et al., 2023). The hazards of these larger eruptions include: i) tsunamis (Carvajal et al., 2022; Lynett et al., 2022; Borrero et al., 2023); ii) pyroclastic density currents or surges that travel over the ocean surface (Carey et al., 1996); iii) submarine volcaniclastic density currents (Seabrook et al., 2023;

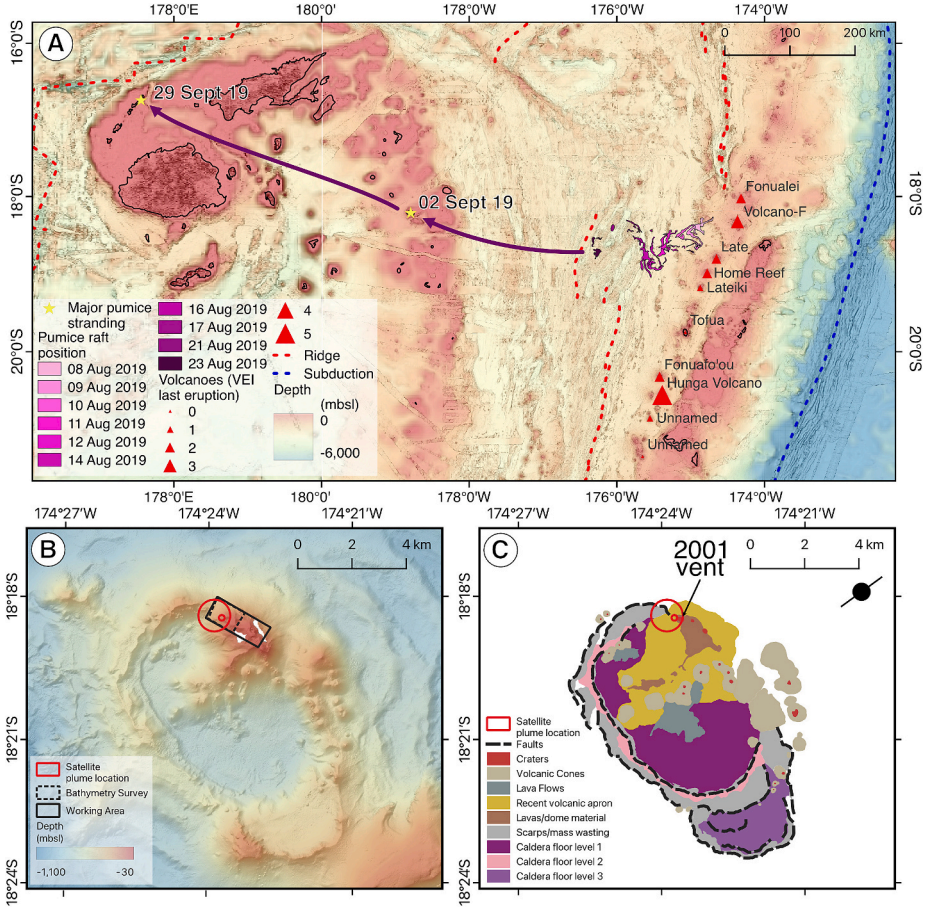

Fig. 1. A) Regional map showing the location of Volcano-F and the other volcanic centres on the northern Tonga-Kermadec Arc. Data from the Global Multi-Resolution Topography Database (Ryan et al., 2009). Volcano symbols are scaled in size by the VEI of their last recorded eruption (Global Volcanism Program, Smithsonian Institution). The 2019 pumice raft dispersal between 8th and 23rd August is shown as mapped by satellites; after the 23rd the raft becomes too dispersed to be easily mapped and its onward path is indicated by the purple arrows. The two yellow stars show the locations of major pumice strandings (where substantial amounts of the pumice raft washed ashore) on Lakeba on the 2nd September and the Northern Yasawa Islands on the 29th September. B) The caldera of Volcano-F showing the shallowest point and associated craters on the northern caldera rim; note the caldera floor is approximately 100 m shallower in the NW sector than the SE sector. The location of the two rings of the 2019 eruption plume observed by Sentinel-2 is shown by the red circles. Dashed line box shows the region covered by bathymetry mapping in this survey (Figs. 2, 3) and the solid line black box shows the approximate full region surveyed and sampled (Fig. 4). Bathymetric data were first published in Brandl et al. (2020), which integrates data from the global GMRT grid (version 3.4 of July 2017: Ryan et al., 2009), RV Southern Surveyor cruise SS2004/11 (Arculus and SS2004/11 shipboard scientists, 2004) and RV Sonne cruise SO-267 (Hannington et al., 2019). C) Geomorphological interpretation by this study of the main caldera features showing the location of faults, young volcanic cones and exposed lavas. The region of most recent activity and a number of volcanic cones appear to form a rough NE – SW orientated ridge (shown by the red dashed line) which closely aligns with the measured regional principle stress orientation shown by the black symbol. (For interpretation of the references to colour in this figure legend, the reader is referred to the web version of this article.)

Clare et al., 2023); and iv) pumice rafts (Bryan et al., 2004, 2012; Jutzeler et al., 2014; Brandl et al., 2020). The 2022 Hunga Volcano eruption generated tsunamis with run up heights of 20 m and large volume submarine volcaniclastic density currents that damaged Tonga's only two subsea telecommunications cables, disconnecting the entire nation from the global internet. To understand how eruptions vary over time at individual volcanoes, and the range and types of hazards posed by caldera systems in this region, it is necessary to characterise the full spectrum of eruptions that occur along the Tofua Arc.

1.2. Caldera cycles and the 2021–2022 eruption of Hunga Volcano

While the eruption of Hunga Volcano was exceptional, the volcano itself is not. On the Tofua Arc north of 22°, at least eight mapped or partially mapped volcanoes have wide (> 1 km) flat-bottomed central craters, usually described as calderas (Fig. 1), that evidence similar, large volume eruptions in the past. Eruptions have been documented at many of these volcanoes but only Hunga Volcano has produced a large (> VEI 4) eruption in recent history. Instead, the other eruptions at these volcanoes have been much less explosive, typically erupting from vents on the shallow sections of caldera rims. Hunga Volcano had experienced several small eruptions in the century preceding the January 2022 event, including 1912 (VEI 2), 1937 (VEI 2), 1988 (VEI 0), 2009 (VEI 2) and 2014/15 (VEI 2) (Vaughan and Webley, 2010; Bohnenstiehl et al., 2013; Colombier et al., 2018; Garvin et al., 2018; Global Volcanism Program, Smithsonian Institution). The 2021/22 eruption of Hunga Volcano was also initially characterised by low VEI eruptive activity during the weeks before the January 2022 climax (Gupta et al., 2022). Thus, smaller eruptions from calderas in the region may occur in isolation, or form patterns of activity that lead up to larger events. It has been suggested that large caldera-forming magmatic systems may follow recurrent evolutionary cycles, including: i) a build-up stage during which magmas accumulate in an upper crustal reservoir (characterised by fewer smaller eruptions of differentiated magmas); ii) a climactic episode during which there is large scale magma withdrawal and caldera collapse; and iii) a post collapse recharge stage characterised by multiple eruptions of less differentiated magmas (Cole et al., 2005). Recent work suggests that this cycle could be shifted, with a caldera cycle ending with the catastrophic eruption and restarting with any magma plumbing system recovery or later eruptions (de Maisonneuve et al., 2021). This perhaps better represents the hazards posed by these systems, as evidence from Santorini caldera in the Mediterranean Sea demonstrates that large explosive volcanic eruptions can occur even early in a recharge phase (Preine et al., 2024). Due to a paucity of sampling, incomplete records of past volcanism, and a lack of monitoring of the majority of the calderas in the Tofua Arc it is unclear if they exhibit such activity cycles or in which stage in a cycle volcanoes may be. Thus, the documentation and characterisation of all eruptions, including those with lower VEIs, are essential to understand the immediate and long-term hazards posed.

1.3. Pumice rafts

Pumice rafts are a common feature of Tofua Arc volcanism (Bryan, 1968; Bryan et al., 2004, 2012) and one of the most disruptive impacts of smaller eruptions. However, it is typically challenging to identify the source volcanoes and formative eruptions as many volcanoes are submerged or only briefly emergent before wave erosion back to below sea level (Hoffmeister et al., 1929; Bryan et al., 2012; Yeo et al., 2022). Pumice rafts can be formed by submarine and subaerial eruptions via a range of eruption styles, including: fallout onto the sea surface from buoyant subaerial eruption columns (Bryan et al., 2012; Vázquez-Prada et al., 2013); entry of subaerial pyroclastic density currents into the sea (Simkin and Fiske, 1984; Jutzeler et al., 2016); shallow submarine dome-forming (Tanakadate, 1935; von Lichtan et al., 2016) or explosive activity (Fiske et al., 1998; Oikawa, 2021); and deep water effusive eruptions (Carey et al., 2018; Manga et al., 2018; but cf. Knafelc et al., 2022). To form a floating raft, a particular combination of magma composition, ascent rate, degassing style, and vent depth is required to produce pumice with sufficient gas bubbles to be buoyant in water (typically >60% porosity, including substantial isolated porosity) and that can arrive at the sea surface without substantial waterlogging during cooling (Kano et al., 1996; Allen et al., 2008; Fauria et al., 2017; Fauria and Manga, 2018; Manga et al., 2018; Mitchell et al., 2021). Floatation of pumice is hypothesised to be promoted by high isolated porosity and narrow pore throats (Mitchell et al., 2021), and the trapping of gas within pore space by water within pore throats (Fauria et al., 2017). Pumice rafts pose a navigational hazard to boats and ships, blocking water intakes for engine cooling systems and abrading vessel hulls. Thus, pumice acts like the maritime equivalent of airborne volcanic ash to aviation, although a significant difference is that it may float for months or years after the eruption, becoming dispersed by currents and winds. Large accumulations of pumice may also inundate ports and harbours and damage coastal infrastructure, particularly fishing equipment and small vessels, and significant amounts of stranded pumice can be remobilised during later storms to form secondary rafts (Yoshida et al., 2022). Pumice raft encounters are becoming more common as society becomes more reliant on shipping for global trade, with at least 20 significant pumice raft events documented in the last 200 years worldwide (Bryan et al., 2012). Pumice rafts may also have biological significance (Jokiel, 1989; Jokiel and Cox, 2003; Bryan et al., 2004, 2012; Velasquez et al., 2018; Roman et al., 2021; Ohno et al., 2022), acting as a long-distance dispersal vector that can rapidly recruit and transport a large biomass and diverse shallow marine communities across open oceans, potentially introducing invasive species to vulnerable locations (Bryan et al., 2012).

1.4. Volcano-F

Volcano-F (also known as Volcano 0403–091 and listed as unnamed volcano number 243091 in the Smithsonian database (Global Volcanism Program, Smithsonian Institution) lies approximately 40 km WNW of the island of Vava'u, Kingdom of Tonga (Fig. 1). Volcano-F was first mapped by the RV Southern Surveyor (expedition SS2004/11 'NoToVE') in 2004. It is a 7 km long by 4 km wide ellipsoidal caldera with multiple preserved caldera floors at 440, 670 and 720 m below sea level (mbsl), surrounded by large (100 s of m wavelength) bedforms that radiate away from the edifice (Fig. 1). Both the existence of the caldera and the bedforms are indicative of large volume eruptions during its geologically-recent history (Pope et al., 2018; Casalbore et al., 2021). Volcano-F reaches its shallowest water depth of 40 mbsl on the northern edge of the caldera, which is also the site of most recent eruptive activity. Volcano-F has had two documented eruptions (VEI 2–2001; VEI 3 – 2019 estimated by Brandl et al. (2020)), which would probably have been missed had they not produced pumice rafts (Bryan et al., 2004). It is possible that other events, particularly those that did not form pumice rafts, have gone unrecorded because of its remote setting. The 2019 eruption had no prior warning and was first noticed when yachts in the region encountered pumice rafts (Sail Surf, 2019) that were tracked back to Volcano-F using satellite images (Brandl et al., 2020; Jutzeler et al., 2020). The eruption occurred between 6th and 8th August (UTC) 2019 (Brandl et al., 2020) and was first imaged by the ESA's Sentinel-2 Satellite (at 22:01 on the 6th August UTC/11:01 on the 7th August local time). The only satellite image that appears to capture the eruption itself shows two concentric rings centred on 18.307°S 174.395°W on the 6th August. Jutzeler et al. (2020) and Brandl et al. (2020) attribute these rings to underwater eruption columns or steam cupolas. No pumice is visible in the whole of the satellite image taken at this time (which is unimpeded by cloud cover), indicating the pumice rafts were produced after this eruption phase. Satellite images recorded by NASA Modis and Aqua satellites (*ESA*, 2019; *NASA*, 2019) track the dispersal of the pumice raft away from the volcano for several weeks. First views of the

pumice raft were available on the 8th August, by which time it had drifted ~35 km west of the vent. The initial pumice raft had an estimated volume of around 30 million m^3, covering 195 km^2 of the ocean (assuming a layer of pumice 15–30 cm thick (Brandl et al., 2020; Jutzeler et al., 2020)). The raft continued drifting westwards towards Fiji with substantial strandings of pumice first on the islands in the Lau Group, before passing through the Koro Sea and impacting coastlines along Viti Levu and islands in the Yasawa Group (Fig. 1). Following pumice strandings in Fiji during early October the pumice continued on to Australia where it began washing up along the Queensland coast in April–May 2020, generally sooner than predictions from numerical models of raft dispersal (Jutzeler et al., 2020).

Volcano-F has at least one other documented eruption, in September 2001. While there was no satellite coverage of the region at the time, on the 28-29th September numerous T-wave signals were detected from the region by the French Polynesian Seismic Network and interpreted to be volcanic and explosive (Global Volcanism Program, Smithsonian Institution, 2001). Pumice rafts thought to be from the eruption were also intercepted in Fiji between the 9th and 25th November 2001. The estimated vent depth for the eruption was less than a few hundred meters, although there was no bathymetric mapping and the vent may have been shallower, consistent with the current summit depth of a few tens of metres. Eyewitness reports suggest an island was formed, though this was likely actually a pumice raft, while an eruption column was observed on the 27th and 28th (Global Volcanism Program, 2002). The eruption appears to have been over by the 1st October, though discoloured water was reported in the region for the entirety of October. The pumice raft reached Australia in October 2002, around one year after the eruption. Pumice clasts were 1–5 cm in diameter, with rare clasts up to 10 cm, and tube pumice was observed, although uncommon. Many clasts were colonised by organisms. Pumices were low-K dacite in composition and had low phenocryst contents, with an assemblage consisting of calcic plagioclase ($An_{88–74}$), pigeonite (En_{45}, Fs_{46}, Wo_9), augite (En_{35}, Fs_{29}, Wo_{36}), and titanomagnetite (Global Volcanism Program, Smithsonian Institution, 2003).

1.5. Aims of this study

Despite being relatively well observed for a moderate (VEI 3) eruption in the region, the eruption of Volcano-F remains relatively poorly characterised in terms of the geochemistry of the erupted products and their formation. We present the results of fast response field survey and sampling <6 months after the 2019 eruption of Volcano-F to provide a unique and detailed case study and to highlight the importance of smaller volcanic eruptions in understanding patterns of activity and hazards posed by this submerged caldera and those elsewhere.

2. Methods

The data collected for this study were part of an urgency response expedition and use a range of small, depth limited equipment, which can be deployed from a small vessel of opportunity. The ROV was depth limited to 100 m (deepest dive 120 m), while sampling equipment needed to be deployed and recovered by hand, thus physically limiting the depths that could be reached. As a result, observations are restricted to the vent region, shallower than 150 m. However, this study also highlights how much is possible with short duration, low-cost projects, where a quick response is required following a shallow submarine event.

2.1. Seafloor mapping and offshore fieldwork

Data and samples were collected from the summit of Volcano-F over five separate days in February 2020 (i.e. five months after the eruption). Positioning was initially guided by previous mapping of the summit following the 2001 eruption and the 6th August Sentinel-2 image (see Fig. 3 of Brandl et al., 2020). On site, positioning was constrained on board by two Raymarine plotters. Bathymetric depth transects (Fig. 2) were collected using single-beam echosounders mounted on the remotely operated vehicle SurfBee (Garmin EchoMap Plus cv) and supplemented by the vessel echosounder (Raymarine Axiom). Bathymetric transects were converted to a grid using the ESRI ArcGIS® Topo to Raster function (Hutchinson, 1989) and bathymetric differencing was carried out in Blue Marble Global Mapper® (Fig. 3). Some artefacts exist in the derived bathymetry as a result of this interpolation, which are discussed in the results. Sampling of eruptive material from the seafloor was conducted in three ways: 1) using a Remotely Operated Vehicle (BlueROV) modified with scoop and claw attachments; 2) a bespoke bucket mini-dredge system (0.4 × 0.6 × 1.0 m) designed and built by the National Oceanography Centre Southampton; and 3) a small Eckman grab-sampler. The dredge and grab sampler were fitted with armoured Go-Pro cameras for sample ground truthing during most deployments. A scale bar was fitted to the Go-Pro camera on the grab samplers and the known dimensions of the equipment in view were used for both the BlueROV and the dredge footage to better constrain dimensions of seafloor features and grain size of imaged deposits. Grab sample locations and ROV tracks are shown in Fig. 4 and representative seafloor images in Fig. 5. Acquired data were projected using Blue Marble Global Mapper® Software and QGIS. A depth and temperature logger (JFE Advantech Co., Ltd.) was mounted on the ROV for all deployments.

Sampling of pumice clasts at the vent was conducted with high spatial resolution. Distinguishing more distal 2019 pumices from those produced from older eruptions is difficult as they are similar in texture, morphology and mineralogy, though some older pumices are encrusted or cemented by bryozoans. Closer to the vent site we are confident pumices were produced by the 2019 eruption because of their size (much larger than those elsewhere), their interlocking nature, the change in the measured bathymetry at the vent and the coverage of many by bacterial mats. These vent proximal samples were primarily selected for analysis. Sampling of stranded raft pumice clasts was carried out on the islands of Lakeba, Fiji (470 km dispersal distance; 3 weeks' float time) and the northern Yasawas, Fiji, (890 km dispersal distance; 6 weeks' float time), and from the Gold Coast in Australia (~3800 km dispersal distance; 4 months' float time). Sampling locations in Fiji were picked from satellite imagery of the stranding events in conjunction with local knowledge of deposit preservation. At each site pumice was collected from at least two randomly positioned 30 × 30 cm quadrats.

2.2. Geochemical methods

Geochemical analyses were conducted using both wavelength dispersive spectrometry (WDS) and X-ray fluorescence spectrometry (XRF) to characterise the geochemistry of the eruption products. All pumice samples were washed multiple times before analysis using Milli-Q in an ultrasonic bath to remove salt and other impurities. Pumice glass was analysed in thin section by WDS using the JEOL JXA 8530f field emission microprobe at Queensland University of Technology. The microprobe is equipped with five wavelength dispersive spectrometers and supported by Probe Software applications (Probe for EPMA, Probe Image and CalcImage; Eugene, OR, United States). Polished thin sections were coated with 20 nm carbon prior to analysis. The following instrument conditions were used for glass analysis: 15 kV accelerating voltage, 10 nA beam current and a 10 μm-defocused beam, with X-ray counts for Si and Na collected first. Detection limits were < 300 ppm for most elements with the exceptions of Ba (500 ppm), F (370 ppm), and Na (380 ppm) for which a 5 s on-peak counting time was used in order to minimize Na loss under the electron beam. Commercially available and in-house natural and synthetic standards were used for calibration. These include Astimex albite (Na), barite (Ba), plagioclase (Al), hematite (Fe), rhodonite (Mn), tugtupite (Cl) and orthoclase (K); NBS synthetic glass standard K411 (Ca, Mg); and in-house celestite (Sr), topaz (F), rutile (Ti), and Lipari glass (Si).

XRF measurements were made following the methods in Sano et al.

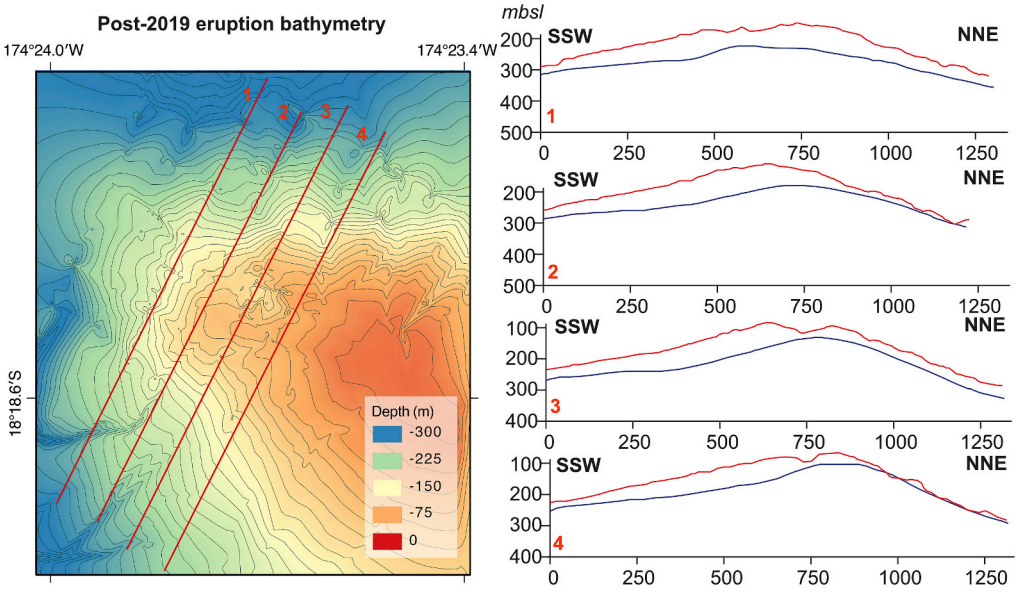

Fig. 2. Profiles across the summit showing the pre-existing profile extracted from the Brandl et al. (2020) bathymetry (blue lines) and the bathymetry collected during this study (red lines). (For interpretation of the references to colour in this figure legend, the reader is referred to the web version of this article.)

(2020). Glasses were washed, crushed to a powder and each sample was pressed into pellets and fused (using tetraborate as a flux) to form glass beads for analysis (pressed pellets giving more accurate measurements of trace elements). Loss on ignition values were determined ahead of analyses by weighing 0.5 g of powder before and after heating (900–1025 °C for 4 h). XRF analyses were carried out on a Rigaku ZSX Primus II at the Division of Mineral Science, Department of Geology and Palaeontology, National Museum of Nature and Science. Details of analytical techniques and calibrations can be found in Sano et al. (2020).

2.3. Clast imaging

X-ray Computed Tomography (XCT) scans were conducted on a selection of representative pumice clasts at the University of Strathclyde on a Nikon XTH 225 LC scanner to characterise the structure and bubble populations of the pumices. Scanning conditions varied across the samples to accommodate a full scan of each clast. For some clasts a higher resolution scan of a region of interest in the centre of the clast was also collected. The accelerating voltage was kept as low as possible (typically 85–95 kV) and the flux maximised for each scan while keeping the spot size on the target smaller that the voxel size following standard acquisition procedures. 3142 projections were collected for all scans, with most requiring a 2 s exposure. In all scans the stop-start scanning acquisition mode was used (i.e. no rotation during collection of each projection) to maximise the visibility of bubble walls in the reconstructed datasets. The raw XCT data were reconstructed using the Nikon propitiatory algorithms, with no additional pre-processing. Where clast geometry required it, multiple scans were collected (vertical offset only, identical acquisition conditions) to capture the entire clast. Smaller samples of similar diameter were loaded into paper tubes for scanning. Optimal resolutions acquired were around 4 μm per pixel. Multiple overlapping scans were collected along the length of each tube and the vertically offset data sets stitched to form a single scan of all clasts. The data were then cropped to produce data volumes containing each clast in isolation. The data volumes were visualised and analysed in Avizo™ 2023.1. The image processing workflow to quantify vesicle X, Y and Z and the internal textures of the clasts was adapted from Yeo et al. (2018). Data were processed using the Avizo software package, where they were imported, orthosliced and greyscale was set to maximise contrast in the images. Interactive thresholding was used to delineate bubbles and a membrane enhancement filter used to help resolve thin glass films. Label analysis was used to measure the cross-sectional area of bubbles in the thresholded images.

3. Results

3.1. Eruption site survey observations

3.1.1. Morphological seafloor changes

Pre-eruption bathymetric data (Brandl et al., 2020) show recent eruption sites were located along a northwest-southeast trending ridge that lies at <100 mbsl and defines the north-eastern margin of the caldera. Bathymetric surveying in 2007 revealed that the highest point along the ridge reached within 40 m of sea level (Global Volcanism Program, Smithsonian Institution, 2007). The bathymetric surveying carried out in 2019 was along single transects, which have been interpolated to create a grid and does not cover the full area of deposits from this eruption. Because of this, interpretations from this map must be made with caution and supported with other observations. There is also a mismatch in resolutions, the pre-eruption data is gridded at 20 m, while our interpolated grid is gridded at 2 m. However, the size of the major features identified exceeds the size of several grid cells in the pre-eruption data and thus changes on this order of magnitude can be considered real. The survey performed during our 2020 expedition identified a new crater centred on 18° 18.454′ S, 174° 23.692′ W, with a diameter of around 80 m and a depth beneath the crater rim of 45 m (Figs. 2, 3). It's presence was confirmed by several ROV dives within it. The location of the new crater aligns closely with the inferred vent location based on the satellite image of an eruption plume (Brandl et al., 2020), which lies to the west of all pre-existing craters identified from the 2018/19 bathymetric survey (Fig. 1B). This new crater lies very close to the likely vent of the 2001 eruption, suggesting little rearrangement between eruptions or during the 2019 event. Differencing of the two datasets (Brandl et al., 2020 and the February 2020 bathymetric survey in this study) shows substantial elevation gain resulting from accumulation of volcanic material across most of the western summit area (Fig. 2, Fig. 3). Based on the 2019 interpolated map, much of this area is now between 10 and 90 m shallower since the eruption, with most deposition located to the southwest of the vent (Fig. 3). Given there are artefacts due to the interpolation algorithm, and a difference in resolution between compared datasets, these differences should be considered estimates. This distribution pattern is consistent with the

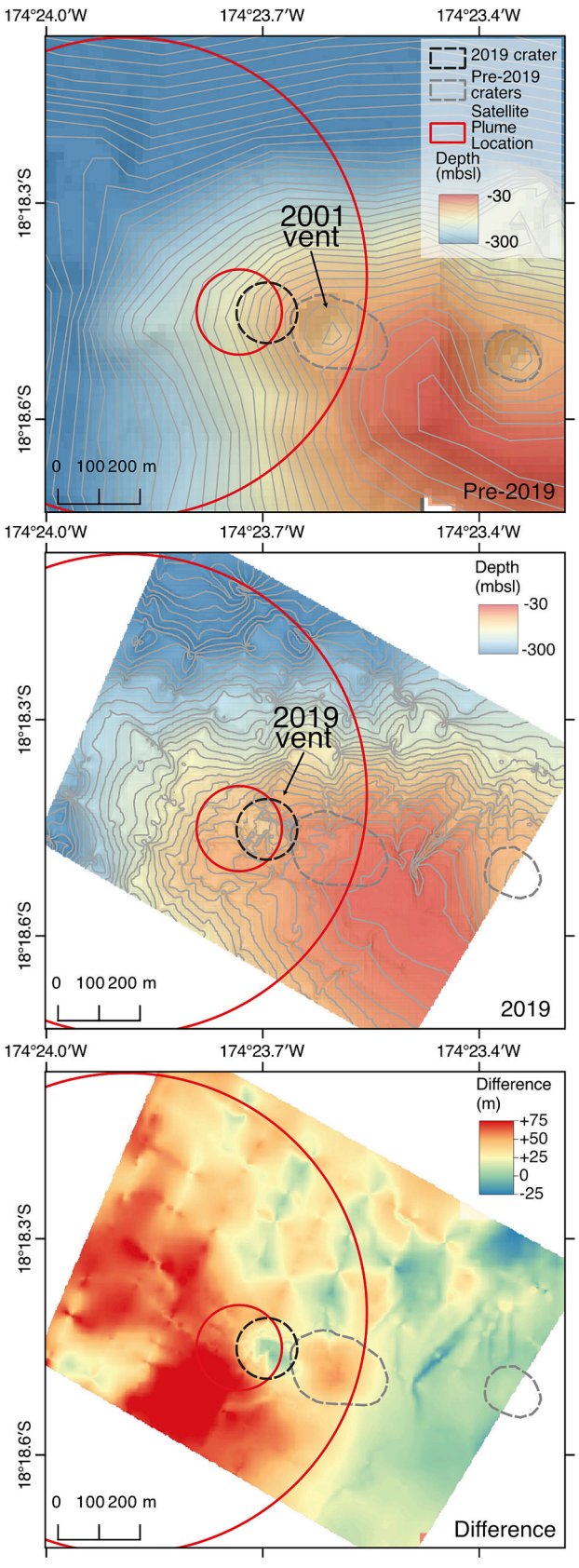

(caption on next column)

Fig. 3. A) Pre-2019 eruption bathymetry of the vent region contoured at 10 m (Brandl et al., 2020). Red circles show the location of the steam rings observed in the satellite imagery. The grey dashed circles show the location of pre-existing crater structures, including the likely source of the 2001 eruption. B) 2020 bathymetry collected during this study for the same region as shown in A contoured at 10 m. The grey dashed circle shows the location of the pre-existing craters and the black dashed circle marks the location of a new crater formed during the 2019 eruption. Red lines show the location of the steam rings observed in the satellite imagery. C) Differencing of the bathymetry shows eruption products primarily distributed to the west of the new crater location.

weather and ocean conditions at the time of the eruption (see fig. S10 of Jutzeler et al., 2020), when the prevailing wind direction was SE to ESE and the prevailing currents go from west to east. The westernmost pre-existing crater (P in Fig. 4B Brandl et al. (2020)) (Fig. 3) is no longer visible in the new bathymetry (Fig. 3B, Fig. 4), suggesting material has been added in this region, although dives in this area did find a small depression remaining, suggesting the interpolation is overestimating the addition of material in this region. The total volumetric increase between the pre- and post-eruption surveys of the vent area is $3.1*10^7$ m^3 bulk volume. While there are artefacts in the interpolated grid, they are within this order of magnitude and this volume represents the best estimate possible with existing data. As the survey also does not cover the entire region across which material was dispersed and deposited, we consider this to be a minimum estimate. If all of this material was pumice, assuming a similar packing density to the raft of 60% (Jutzeler et al., 2014; Brandl et al., 2020) and using an average measured porosity for the seafloor clasts of 70%, this would have a dense rock equivalent (DRE) of $5.6*10^6$ m^3.

3.1.2. *Distribution of eruptive products*

Representative images from the grab sampler deployments and the ROV dives are shown in Fig. 5. Exposed, likely older, lavas are observed over the entire surveyed area, only locally concealed by unconsolidated pyroclastic material. While it was not surveyed in its entirety, the top of this pinnacle, which is the shallowest point on the volcano and seems to be the focus of recent volcanic activity, forms a fairly flat plateau about 1.5 km across characterised by at least three pit craters aligned roughly east-west (Fig. 1B); the most westerly of which (Fig. 3) formed during the 2019 eruption, most likely as a result of the slight relocation of the 2001 vent (Global Volcanism Program, Smithsonian Institution, 2007) and infilling of the 2001 vent location (for more detailed bathymetry see Supplementary File 1). The seabed facies identified from seafloor video appear to reflect proximal to distal relationships from the 2019 eruption. The most distal areas from the vent (Fig. 5A, B, C), >1 km from the active vent and in water depths between 30 and 100 m, are characterised by symmetric ripples (Fig. 5B) of moderately sorted (~1–3 cm diameter) mobile pumice clasts (Fig. 5A). On the slopes of the caldera rim the pumice clasts are slightly larger and better sorted (Fig. 5D). Between 100 and 1000 m from the 2019 vent (Fig. 5 E, F, G, H), the clasts are generally more poorly sorted and coarser, increasing in size towards the 2019 vent (Fig. 5E; Fig. 6 A,B), where loose clasts commonly reach 30 cm. There also appears to be a general increase in clast size towards all the pit craters. Lavas are still visible (Fig. 5E) but bedforms were not as clearly defined as in distal regions, despite lying at similar water depths, probably due to the overall coarser material that is not so readily mobilised. The edge of the 2019 vent crater lies around 75 mbsl and reaches depths of 120 mbsl in its centre (Fig. 2). This region is characterised by chaotic, poorly sorted piles of large pumice blocks (typically 0.5–30 cm but commonly reaching 1 m in diameter) and lavas were no longer visible (Fig. 5 J, K, L), presumably buried beneath the pumices. Most large blocks are thought to be pumice, as they could be easily moved by the small ROV indicating near-neutral buoyancy, though some may also be lavas or scorias, produced during the eruption (Fig. 5 J, K). There is no evidence of wave-related bedforms, probably because of the larger pumice clast sizes and the relatively recent deposition of the

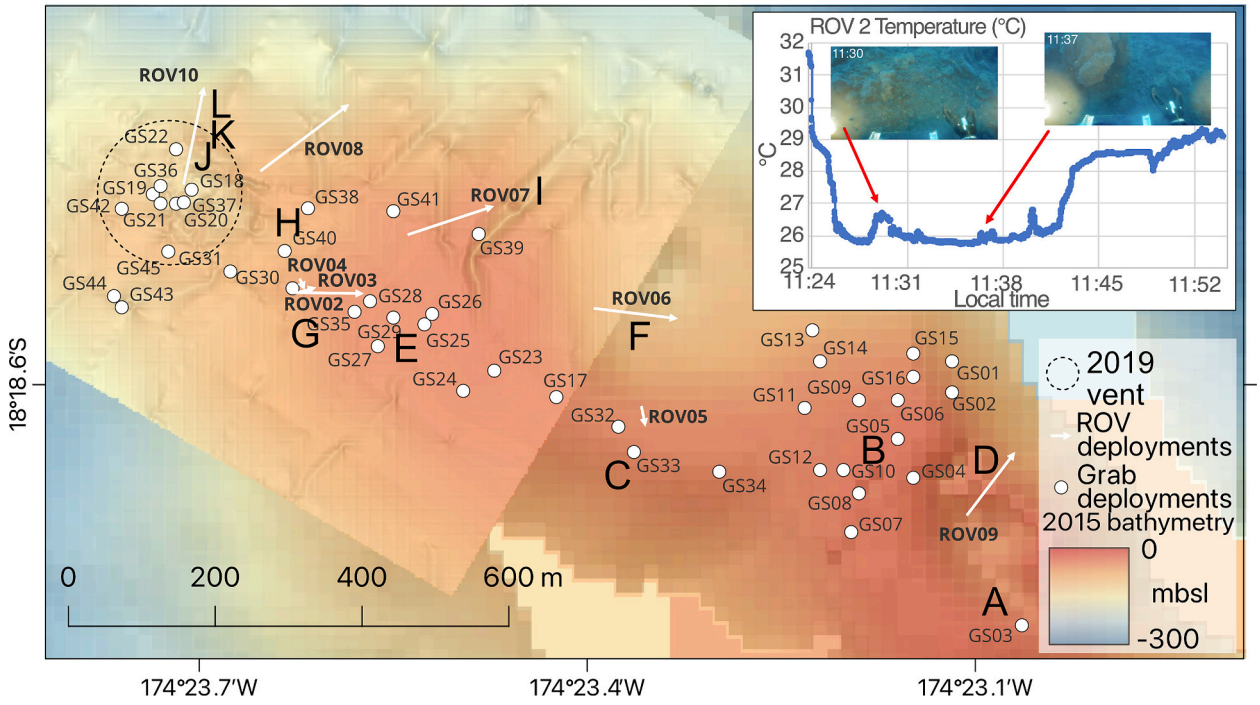

Fig. 4. Combined bathymetric map showing data from Brandl et al. (2020) (darker colours) and this study (brighter colours) showing the grab sampler locations and ROV tracks from this field survey. Inset: Temperature data from ROV dive 2 showing detected temperature anomalies and the corresponding ROV video imagery, revealing their association with regions of bacterial mats. The temperature data were collected along the ROV02 path, however absolute navigational positioning is not available from the Blue ROV deployments so they cannot be precisely positioned. (For interpretation of the references to colour in this figure legend, the reader is referred to the web version of this article.)

material surveyed.

3.1.3. *Bacterial mats, alteration and temperature anomalies*

No seafloor alteration was observed in the distal regions >1 km from the vent. Between 100 and 100 m from the vent patches of hydrothermal alteration were observed (Fig. 5 G, H), indicating this area was impacted by the eruption and experienced fluid flow during or directly after it. The only temperature anomalies observed from temperature measurements, which were up to 0.5 °C above ambient levels, also occurred in this area (Fig. 4B), suggesting some ongoing outflow in February 2020. The ROV dive footage reveals that these anomalies occurred above areas of seafloor that were covered by widespread bacterial mats (Fig. 4B). In the newest vent region, white and orange staining on the seafloor is common (Fig. 5 L) though temperature anomalies were not measured.

3.1.4. *Impacts on seafloor ecosystems*

>1 km from the vent a number of sessile (primarily sponges, bryozoans and corals) and mobile (spider conches, gastropods, moray eels) organisms were seen in video footage (Fig. 5C), suggesting this region was relatively undisturbed by the 2019 eruption (Fig. 6C). Between 100 and 1000 m from the vent, the region was mostly devoid of the sessile fauna seen in distal regions (Fig. 6C). The vent region is completely devoid of sessile fauna, as would be expected soon after the eruption.

3.2. *2019 Eruption Pumice Geochemistry*

We present the first major and trace element data set for the floating and sunken products of the 2019 eruption (Tables 1, 2). Chemical analyses of individual pumice clasts were undertaken to: i) characterise the eruptive products and magma chemistry to evaluate if any chemical differences exist between pumice that entered the pumice raft and pumice that sunk and remained at the vent; ii) confirm via chemical similarity that pumice material beached along eastern Australia in 2020 was the same as the pumice rafts collected from strand deposits in Fiji in September 2019 and within a few days of raft formation; and iii) evaluate chemical similarity, or lack thereof, with the 2001 eruption as a basis for interpreting whether the 2019 eruption records a new magma recharge event in the volcano. Whole-clast and pumice glass compositions are given in Tables 1 and 2.

The 2019 pumice compositions are dacitic (cf. Jutzeler et al., 2020), in keeping with the notable paucity of andesite and rhyolite erupted in the Tofua Arc (Fig. 7A). The low-K dacite whole-clast and glass compositions (Tables 1, 2) are therefore consistent with magma compositions in the 2001 eruption from the same volcano (Bryan et al., 2004) and from other silicic explosive eruptions in the Tofua arc more generally (e.g., Fig. 7). However, dacitic lavas from Fonualei (Turner et al., 2012; Beier et al., 2017) are calc-alkalic (Fig. 7A).

The chemical similarity between pumice from the 2019 and 2001 eruptions of Volcano-F (Bryan et al., 2004) indicates that the magmas are likely related. For the 2019 erupted products, whole-pumice compositions from the raft are near identical to sunken pumice at the vent (Table 1). However, glass compositions are slightly more silicic than whole pumice compositions (Fig. 8), possibly as a result of the crystal cargo in the pumice. Raft pumice glass compositions are slightly less silicic than seafloor pumice glass compositions and have relatively higher MgO and CaO and lower K_2O contents (Fig. 8). This indicates a subtle geochemical difference between raft pumice and near-vent sunken pumice (Table 1) and further study is required to determine if this chemical difference is a factor for why some pumice has sunk and remained at the vent while other pumice remained buoyant and was dispersed widely from the volcano.

A growing body of geochemical data now exists for pumice rafts sourced from eruptions over the last 100 years in Tonga (Fig. 7). When analysed, almost all the pumice that produces large, long-lived pumice rafts is dacite, but different eruptions and their source volcanoes can be discriminated based on minor and trace elements. For example, TiO_2 K_2O and P_2O_5 appear to be useful discriminators of different eruptions (Fig. 7C). Dacites erupted at the northern end of the Tofua arc from

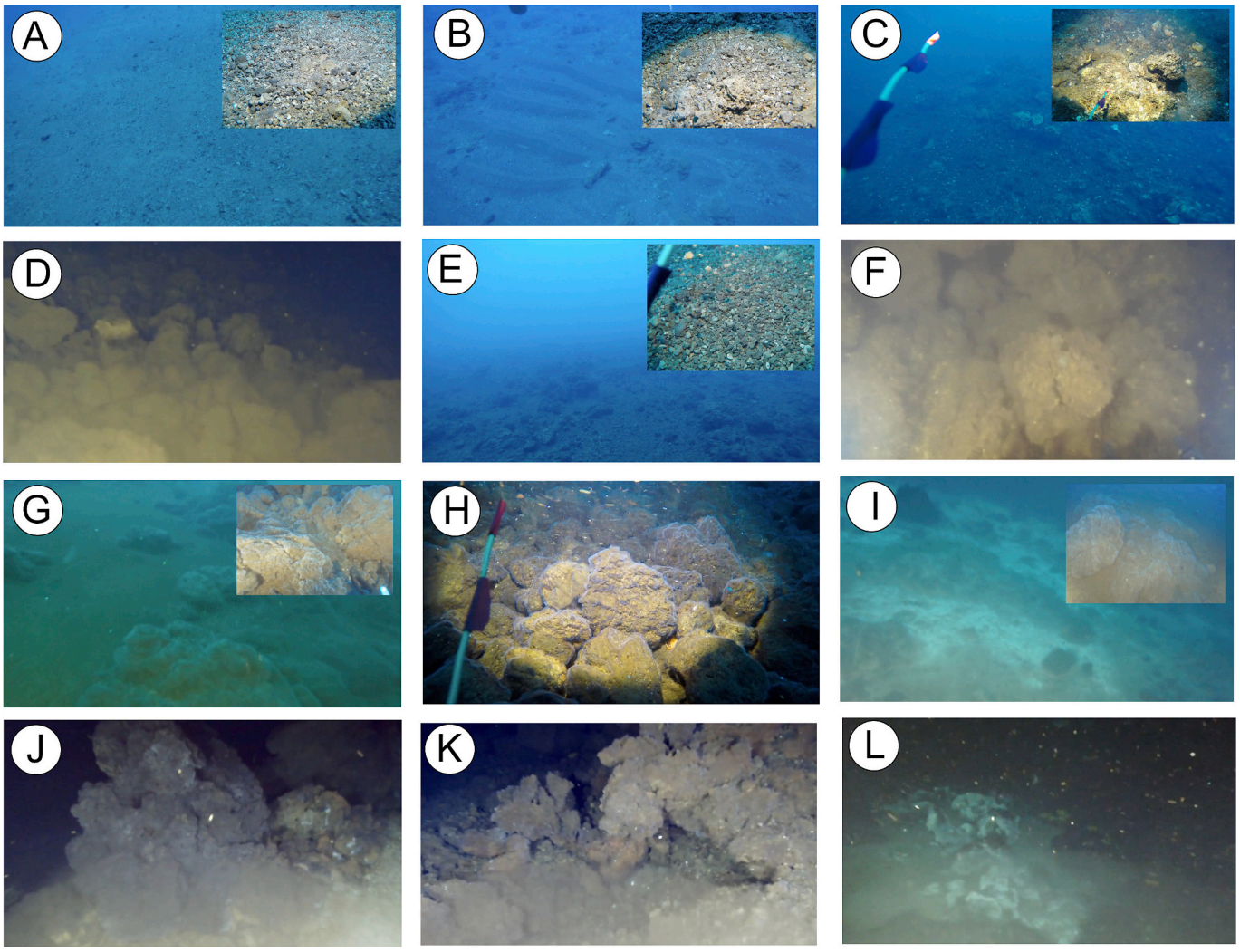

Fig. 5. Representative stills taken from the grab sampler camera and the ROV during deployments. Insets show close ups of seafloor material where these were available. Broad field of view typically 2–3 m. Where visible the taped divisions on the camera are 1 cm. Locations of photos correspond to letters in Fig. 4. [A] Distal reworked dark and light grey pumices; [B] Thin layer of reworked pumices overlying older lavas with symmetric ripples; [C] Lavas and pumices on the southern slope of the caldera rim; [D] Pumice clasts up to 10 cm on the northern slope of the caldera rim; [E] Reworked dark and light gey pumices to the east of the likely 2001 vent; [F] Pumice clasts up to 10 cm in an older crater; [G] Lavas and pumices east of the 2001 and 2019 vents showing bacterial mat coverage; [H] Pumice clasts 10–15 cm in diameter in the location of the likely 2001 eruption vent site covered with bacterial mats; [I] Bacterial mats on lavas and pumices on the northern slope of the caldera rim; [J] Large pumices up to 1 m in diameter with bacterial mat coverage in the vent of the 2019 eruption; [K] Large pumices up to 50 cm in diameter with bacterial at coverage on the northern slope of the 2019 vent crater; [L] Bacterial mats on the northern edge of the 2019 vent crater.

Fonualei (Turner et al., 2012) have the highest K_2O contents, while dacites from Eua (Bryan et al., 1972) and the 1968 Metis Shoal eruption have the lowest TiO_2 contents, suggesting some non-systematic along arc-variation. The dacitic pumice from the 1928 "Falcon" (now known as Fonuafo'ou) eruption (Hoffmeister et al., 1929; Lacroix, 1939) are also geochemically distinct. Recent eruptions from Volcano-F are distinctive in being characterised by TiO_2 contents between ~0.55–0.6 wt% (Table 1). In contrast, similar dacite pumice raft-producing eruptions from the nearby Home Reef volcano that erupted in 1984 and 2006 are characterised by slightly higher TiO_2 (~0.63–0.7 wt%), K_2O (~0.9 wt%) and P_2O_5 (~0.2–0.22 wt%) contents. Of note is the similarity between raft pumice collected in 1964 (Ewart et al., 1998), following an unobserved eruption, and 2001 and 2019 pumice compositions from Volcano-F (Fig. 7). The chemical similarity of the 1964 pumice raises the possibility Volcano-F had a third eruption in the last 60 years attesting that this volcano is significantly at unrest.

3.3. Phenocryst mineralogy

Pumices from the 2019 eruption contain, in order of relative abundance, phenocrysts of bytownite ($An_{86–70}$), augite ($En_{35}Fs_{30}Wo_{35}$), orthopyroxene/pigeonite ($En_{45}Fs_{45}Wo_{10}$), and titanomagnetite. The average pyroxene compositions are the same as observed in the 2001 eruption, whereas plagioclase compositions are slightly less calcic (Bryan et al., 2004). Phenocrysts usually occur in small glomerocrystic aggregates. Equilibrium tests (Putirka, 2008) for the clinopyroxene and pigeonite phenocrysts including those from glomerocrysts fail suggesting the co-existing pyroxenes are not in equilibrium and are antecrystic.

3.4. Pumice characteristics

In hand specimen, samples collected from the floating raft and the seafloor do not exhibit clear banding but do display textural variation, even on very small (mm) scales. Individual analysis and classification of the entire collected quadrat samples suggests a significant proportion (25–50%) of the clasts that floated and were stranded are characterised

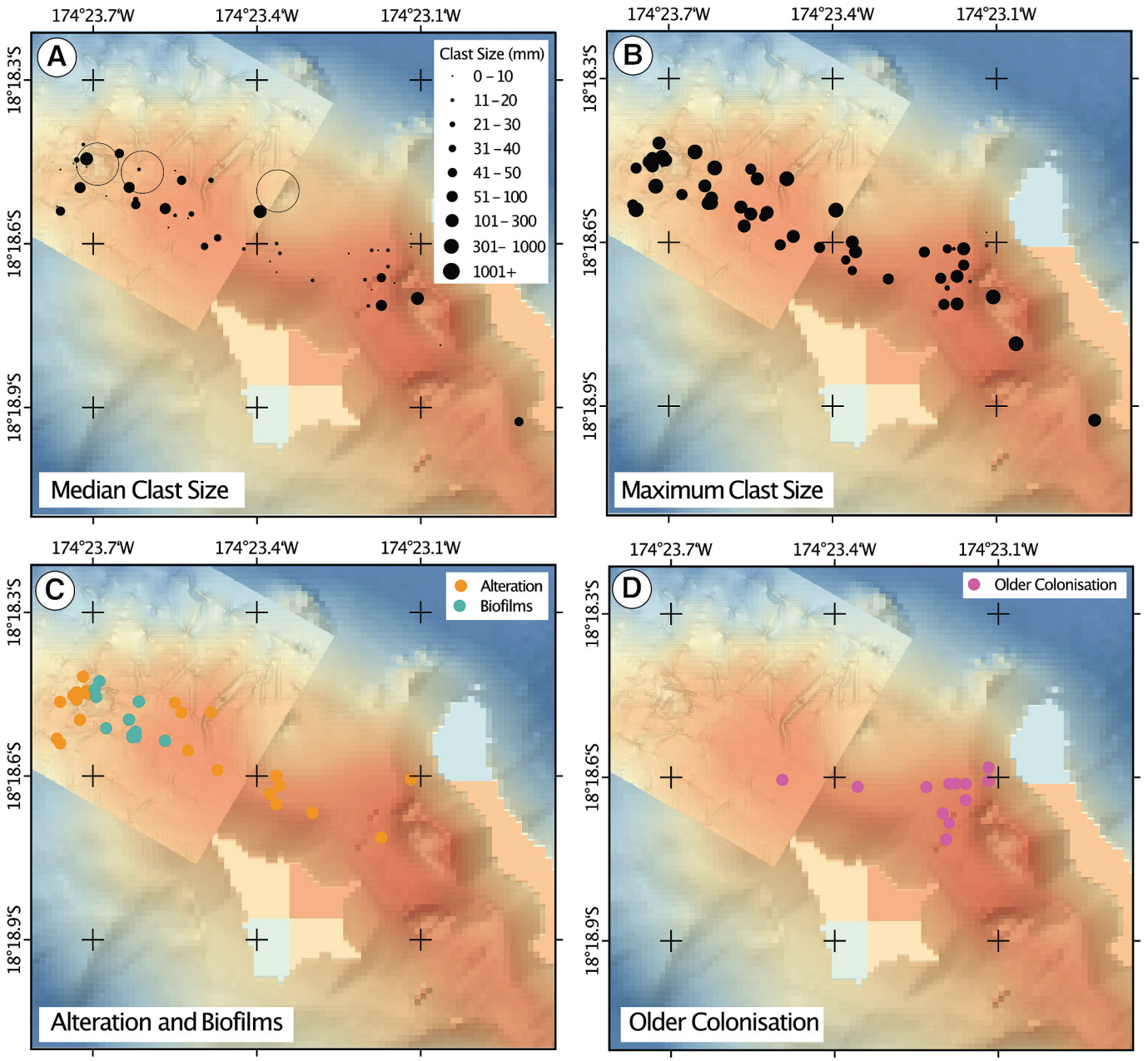

Fig. 6. Observations from grab sampler and ROV video of [A&B] clast sizes (at the same scale) and approximate locations of new and pre-existing craters (grey circles); [C] locations of bacterial mats (biofilms) and alteration; [D] locations of colonisation by sessile fauna overlaid on the pre-erutpion bathymetry from Brandl et al. (2020) (darker colours) and this study (brighter colours).

by a domain of very glassy, apparently slightly lower and/or more sheared porosity and variably-developed bark-like texture on one or more surfaces. The sunken material contained fewer such clasts, although smaller sample sizes make direct comparison difficult. These bark textured sections of samples contained bubbles that were more sheared than the rest of the sample, consistent with the idea that they cooled rapidly on eruption. These conditions, fast quenching and high shear, may encourage the development of small pore throats that promote flotation (Fauria et al., 2017; Mitchell et al., 2021), however further work is required to prove this.

The XRCT data (Fig. 9) reveal a range of shapes and textures in the raft pumice samples. Bread crust textures were observed on some pumice clasts (Fig. 9 A&B) but the majority of samples had smoother surface textures, sometimes with one surface displaying a sheared, glassy bark-like texture, likely associated with rapid chilling of a deforming magma. Scans show that these sections are denser with fewer bubbles (Fig. 9 E&F) and the bubble density increases away from these boundaries. There is no clear trend in bubble-size distributions or bubble size gradation towards the clast margins in samples without these margins. Samples of floating and sunken pumice all have bulk porosities of between 60 and 72%. Most bubbles have cross sectional areas of <40 μm (Fig. 9 I), but some constitute larger volumes. Bubble shapes range from close to round to elongate textures produced by deformation and irregular shapes likely resulting from coalescence. The XRCT scans also show regions of a denser material, forming bands and swirls not recognisable in hand specimen. These resemble mingling textures (Fig. 9 G, H), which can be sheared into bands by deformation (Fig. 9 F).

Table 1
XRF analyses (bulk rock) of samples collected for this study.

Sample ID	TNGA01	TNGA072	TNGA02	TNGA03	TNGA04	TNGA05	TNGA06	TNGA07	TNGA08	TNGA09	TNGA021	SSR	TNGA10	TNGA11							BB-2020-01
Sample Name	DR02	DR03	DR04	DR05	DR06	ROV02	ROV04	ROV09	ROV10	GS38	GS16	SSR1	Lakeba-Nukunuku Beach	Lakeba-Tubou Guesthouse	FIJI-NAV	FIJI-NAV-02	FIJI-VAT-03	FIJI-NUKU-02	FIJI-TUB-03	FIJI-WACI-02	QLD-0403-091
Sample Method	Dredge	Dredge	Dredge	Dredge	Dredge	ROV	ROV	ROV	ROV	Grab sample	Grab sample	Ocean surface	Beach strand	Beach strand	Beach strand	Beach strand	Beach strand	Beach strand	Beach strand	Beach strand	Beach strand
Pumice Source	Seafloor	Seafloor	Seafloor	Seafloor	Seafloor	Seafloor	Seafloor	Seafloor	Seafloor	Seafloor	Seafloor	Raft	Raft	Raft	Raft	Raft	Raft	Raft	Raft	Raft	Raft
Country	Tonga	Tonga	Tonga	Tonga	Tonga	Tonga	Tonga	Tonga	Tonga	Tonga	Tonga	Tonga	Fiji	Fiji	Fiji	Fiji	Fiji	Fiji	Fiji	Fiji	Australia
Grid Reference												S18° 55.129' W175° 21.266'									
Wt%																					
SiO_2	65.32	65.16	65.44	65.36	65.22	65.29	65.28	65.45	65.15	65.29	65.10	65.19	65.27	65.01	65.25	64.62	65.25	65.25	64.83	65.13	65.22
TiO_2	0.57	0.57	0.56	0.57	0.57	0.57	0.57	0.56	0.57	0.57	0.57	0.57	0.56	0.57	0.57	0.56	0.57	0.56	0.56	0.57	0.57
Al_2O_3	12.86	12.88	12.85	12.84	12.85	12.86	12.91	12.82	12.92	12.87	12.89	12.84	12.87	12.88	12.87	12.76	12.88	12.84	12.80	12.91	12.88
Fe_2O_3T	10.12	10.20	10.13	10.16	10.15	10.16	10.14	10.14	10.20	10.12	10.32	10.20	10.10	10.11	10.13	10.08	10.10	10.16	10.05	10.17	10.17
MnO	0.19	0.18	0.19	0.19	0.19	0.19	0.19	0.19	0.19	0.19	0.19	0.19	0.19	0.19	0.19	0.19	0.19	0.19	0.19	0.19	0.19
MgO	1.40	1.61	1.39	1.42	1.43	1.41	1.43	1.39	1.44	1.41	1.52	1.43	1.42	1.45	1.44	1.53	1.44	1.44	1.44	1.45	1.41
CaO	5.99	5.93	5.93	5.92	6.03	6.00	6.00	5.92	6.03	6.00	5.89	6.06	5.99	6.28	6.02	6.03	6.02	5.99	6.66	6.04	6.03
Na_2O	2.74	2.74	2.75	2.74	2.77	2.73	2.72	2.73	2.73	2.74	2.77	2.73	2.81	2.75	2.72	3.38	2.75	2.75	2.68	2.77	2.73
K_2O	0.67	0.59	0.63	0.66	0.65	0.65	0.62	0.66	0.64	0.67	0.60	0.65	0.64	0.64	0.67	0.72	0.66	0.68	0.66	0.64	0.65
P_2O_5	0.14	0.14	0.14	0.14	0.14	0.14	0.14	0.14	0.14	0.14	0.14	0.14	0.14	0.14	0.14	0.14	0.14	0.14	0.14	0.14	0.14
Raw Total	100.48	100.93	100.49	100.75	100.15	100.53	100.87	100.62	100.49	100.69	100.61	100.03	100.45	100.19	100.77	100.14	100.38	100.83	100.71	100.79	100.39
LOI	0.52	0.11	0.97	0.21	0.54	0.35	0.30	0.40	3.69	0.51	0.12	2.09	1.20	1.40	0.59	1.43	1.69	1.02	1.17	0.97	0.58
ppm																					
V	82.75	72.59	82.51	74.93	82.52	80.77	83.04	80.62	92.15	84.58	76.14	88.09	81.11	88.65	81.86	80.52	88.71	80.30	84.69	84.44	82.74
Cr	3.64	3.40	3.48	2.60	3.82	3.47	3.15	2.82	3.72	2.27	4.93	2.46	2.81	3.19	3.59	3.34	3.94	4.70	2.60	3.58	4.03
Co	29.21	28.58	29.75	28.45	29.12	29.03	28.83	29.08	30.24	29.29	29.03	29.82	28.95	29.43	29.28	27.84	29.94	29.50	28.70	29.54	29.33
Cu	48.52	88.05	92.99	73.37	53.30	48.49	64.43	96.95	81.84	54.84	87.03	51.09	50.30	71.33	51.20	47.33	64.24	48.11	55.16	56.64	61.68
Zn	103.64	109.15	106.75	105.52	104.14	104.25	104.44	107.23	105.57	103.77	107.46	104.52	103.32	105.66	105.96	103.01	106.37	105.72	104.14	105.41	106.81
Rb	9.47	9.08	9.47	9.35	9.40	9.47	9.33	9.56	9.20	9.38	9.30	9.42	9.52	9.32	9.43	10.82	9.53	9.33	9.03	9.60	10.01
Sr	212.87	215.35	211.12	214.40	213.37	213.76	211.67	211.98	209.63	211.44	214.50	213.04	211.41	240.01	215.29	213.97	212.74	212.34	282.46	212.53	214.01
Y	23.22	23.40	22.77	23.59	22.89	23.25	22.90	22.94	22.80	22.99	23.42	23.19	23.04	22.75	23.08	22.13	22.70	22.96	22.65	22.66	23.08
Zr	37.60	38.44	37.56	38.20	37.54	37.94	37.34	37.64	36.96	37.26	38.67	36.77	37.32	40.20	38.03	37.51	37.59	37.72	44.39	37.52	39.06
Nb	3.58	3.62	3.45	3.70	3.52	3.60	3.57	3.54	3.50	3.57	3.67	4.69	3.58	3.49	3.49	3.47	3.47	3.55	3.40	3.49	3.57
Ba	159.28	158.18	160.31	160.18	160.83	163.62	157.08	165.64	157.76	154.88	158.81	155.33	157.01	156.03	164.42	157.18	156.44	158.43	155.37	163.89	160.33
Pb	3.60	3.95	4.31	3.74	3.53	4.11	3.54	3.60	4.50	3.79	3.98	3.43	3.69	3.83	3.72	3.68	3.88	3.79	3.89	3.98	3.65
Ce	7.59	7.51	9.09	11.08	8.93	7.78	6.34	5.88	9.17	9.53	9.19	10.17	5.94	7.98	9.35	8.01	7.50	9.13	4.00	7.36	8.24
Th	0.85	0.85	0.70	0.74	0.66	0.42	0.73	0.64	0.28	0.83	0.59	0.68	0.74	0.51	0.64	0.79	0.86	0.89	0.76	0.46	0.75

Sample Name	DR02	DR03	DR04	DR05	DR06	ROV02	ROV04	ROV09	ROV10	GS38	GS16	SSR1	Lakeba-Nuku1	Lakeba-Tub1	Yasawa-Nav1	Yasawa-Nav2	Yasawa-Vat1	Lakeba-Nuku2	Lakeba-Tub2	Lakeba-Waci1	QLD-0403-091
Sample Method	Dredge	Dredge	Dredge	Dredge	Dredge	ROV	ROV	ROV	ROV	Grab sample	Grab sample	Ocean surface	Beach strand	Beach strand	Beach strand	Beach strand	Beach strand	Beach strand	Beach strand	Beach strand	Beach strand
Country	Tonga	Tonga	Tonga	Tonga	Tonga	Tonga	Tonga	Tonga	Tonga	Tonga	Tonga	Tonga	Fiji	Fiji	Fiji	Fiji	Fiji	Fiji	Fiji	Fiji	Australia
Wt%																					
SiO_2	65.32	65.16	65.44	65.36	65.22	65.29	65.28	65.45	65.15	65.29	65.10	65.19	65.27	65.01	65.25	64.62	65.25	65.25	64.83	65.13	65.22
TiO_2	0.57	0.57	0.56	0.57	0.57	0.57	0.57	0.56	0.57	0.57	0.57	0.57	0.56	0.57	0.57	0.56	0.57	0.56	0.56	0.57	0.57

(*continued on next page*)

Table 1 (*continued*)

Sample Name	DR02	DR03	DR04	DR05	DR06	ROV02	ROV04	ROV09	ROV10	GS38	GS16	SSR1	Lakeba-Nuku1	Lakeba-Tub1	Yasawa-Nav1	Yasawa-Nav2	Yasawa-Vat1	Lakeba-Nuku2	Lakeba-Tub2	Lakeba-Waci1	QLD-0403-091
Sample Method	Dredge	Dredge	Dredge	Dredge	Dredge	ROV	ROV	ROV	ROV	Grab sample	Grab sample	Ocean surface	Beach strand	Beach strand	Beach strand	Beach strand	Beach strand	Beach strand	Beach strand	Beach strand	Beach strand
Country	Tonga	Tonga	Tonga	Tonga	Tonga	Tonga	Tonga	Tonga	Tonga	Tonga	Tonga	Tonga	Fiji	Fiji	Fiji	Fiji	Fiji	Fiji	Fiji	Fiji	Australia
Al_2O_3	12.86	12.88	12.85	12.84	12.85	12.86	12.91	12.82	12.92	12.87	12.89	12.84	12.87	12.88	12.87	12.76	12.88	12.84	12.80	12.91	12.88
Fe_2O_3T	10.12	10.20	10.13	10.16	10.15	10.16	10.14	10.14	10.20	10.12	10.32	10.20	10.10	10.11	10.13	10.08	10.10	10.16	10.05	10.17	10.17
MnO	0.19	0.18	0.19	0.19	0.19	0.19	0.19	0.19	0.19	0.19	0.19	0.19	0.19	0.19	0.19	0.19	0.19	0.19	0.19	0.19	0.19
MgO	1.40	1.61	1.39	1.42	1.43	1.41	1.43	1.39	1.44	1.41	1.52	1.43	1.42	1.45	1.44	1.53	1.44	1.44	1.44	1.45	1.41
CaO	5.99	5.93	5.93	5.92	6.03	6.00	6.00	5.92	6.03	6.00	5.89	6.06	5.99	6.28	6.02	6.03	6.02	5.99	6.66	6.04	6.03
Na_2O	2.74	2.74	2.75	2.74	2.77	2.73	2.72	2.73	2.73	2.74	2.77	2.73	2.81	2.75	2.72	3.38	2.75	2.75	2.68	2.77	2.73
K_2O	0.67	0.59	0.63	0.66	0.65	0.65	0.62	0.66	0.64	0.67	0.60	0.65	0.64	0.64	0.67	0.72	0.66	0.68	0.66	0.64	0.65
P_2O_5	0.14	0.14	0.14	0.14	0.14	0.14	0.14	0.14	0.14	0.14	0.14	0.14	0.14	0.14	0.14	0.14	0.14	0.14	0.14	0.14	0.14
Raw Total	100.48	100.93	100.49	100.75	100.15	100.53	100.87	100.62	100.49	100.69	100.61	100.03	100.45	100.19	100.77	100.14	100.38	100.83	100.71	100.79	100.39
LOI	0.52	0.11	0.97	0.21	0.54	0.35	0.30	0.40	3.69	0.51	0.12	2.09	1.20	1.40	0.59	1.43	1.69	1.02	1.17	0.97	0.58
ppm																					
V	82.75	72.59	82.51	74.93	82.52	80.77	83.04	80.62	92.15	84.58	76.14	88.09	81.11	88.65	81.86	80.52	88.71	80.30	84.69	84.44	82.74
Cr	3.64	3.40	3.48	2.60	3.82	3.47	3.15	2.82	3.72	2.27	4.93	2.46	2.81	3.19	3.59	3.34	3.94	4.70	2.60	3.58	4.03
Co	29.21	28.58	29.75	28.45	29.12	29.03	28.83	29.08	30.24	29.29	29.03	29.82	28.95	29.43	29.28	27.84	29.94	29.50	28.70	29.54	29.33
Cu	48.52	88.05	92.99	73.37	53.30	48.49	64.43	96.95	81.84	54.84	87.03	51.09	50.30	71.33	51.20	47.33	64.24	48.11	55.16	56.64	61.68
Zn	103.64	109.15	106.75	105.52	104.14	104.25	104.44	107.23	105.57	103.77	107.46	104.52	103.32	105.66	105.96	103.01	106.37	105.72	104.14	105.41	106.81
Rb	9.47	9.08	9.47	9.35	9.40	9.47	9.33	9.56	9.20	9.38	9.30	9.42	9.52	9.32	9.43	10.82	9.53	9.33	9.03	9.60	10.01
Sr	212.87	215.35	211.12	214.40	213.37	213.76	211.67	211.98	209.63	211.44	214.50	213.04	211.41	240.01	215.29	213.97	212.74	212.34	282.46	212.53	214.01
Y	23.22	23.40	22.77	23.59	22.89	23.25	22.90	22.94	22.80	22.99	23.42	23.19	23.04	22.75	23.08	22.13	22.70	22.96	22.65	22.66	23.08
Zr	37.60	38.44	37.56	38.20	37.54	37.94	37.34	37.64	36.96	37.26	38.67	36.77	37.32	40.20	38.03	37.51	37.59	37.72	44.39	37.52	39.06
Nb	3.58	3.62	3.45	3.70	3.52	3.60	3.57	3.54	3.50	3.57	3.67	4.69	3.58	3.49	3.49	3.47	3.47	3.55	3.40	3.49	3.57
Ba	159.28	158.18	160.31	160.18	160.83	163.62	157.08	165.64	157.76	154.88	158.81	155.33	157.01	156.03	164.42	157.18	156.44	158.43	155.37	163.89	160.33
Pb	3.60	3.95	4.31	3.74	3.53	4.11	3.54	3.60	4.50	3.79	3.98	3.43	3.69	3.83	3.72	3.68	3.88	3.79	3.89	3.98	3.65
Ce	7.59	7.51	9.09	11.08	8.93	7.78	6.34	5.88	9.17	9.53	9.19	10.17	5.94	7.98	9.35	8.01	7.50	9.13	4.00	7.36	8.24
Th	0.85	0.85	0.70	0.74	0.66	0.42	0.73	0.64	0.28	0.83	0.59	0.68	0.74	0.51	0.64	0.79	0.86	0.89	0.76	0.46	0.75

Table 2
WDS analyses (pumice glasses) of samples collected for this study.

SAMPLE	GSO4-a4-1	GSO4-a6-1	GSO4-a6.5-1	GSO4-a6.5-1A	GSO4-1	GSO4-a7-1	GSO4-a7-2	GSO4-a8-1	GSO4-a8-1a	GSO4-a8-1b	GSO4-a8-1c	GSO4-a9-1a	GSO4-a9-1b	GSO4-a10-1	GSO4-a11-1a	GSO4-a11-1b	GSO4-a13-1a	GSO4-a13-1b	GSO4-a15-1	GSO16-a4-1	GSO16-a5-1
Sample Method	Grab Sample	Grab Sample	Grab Sample	Grab Sample	Grab Sample	Grab Sample	Grab Sample	Grab Sample	Grab Sample	Grab Sample	Grab Sample	Grab Sample	Grab Sample	Grab Sample	Grab Sample	Grab Sample	Grab Sample	Grab Sample	Grab Sample	Grab Sample	Grab Sample
Pumice Source	Seafloor	Seafloor	Seafloor	Seafloor	Seafloor	Seafloor	Seafloor	Seafloor	Seafloor	Seafloor	Seafloor	Seafloor	Seafloor	Seafloor	Seafloor	Seafloor	Seafloor	Seafloor	Seafloor	Seafloor	Seafloor
wt %																					
SiO_2	68.92	68.20	67.54	68.27	67.56	68.37	67.17	67.89	68.84	67.96	67.93	69.55	67.02	68.05	67.43	68.63	68.67	68.73	68.76	67.43	67.87
TiO_2	0.53	0.55	0.54	0.49	0.50	0.50	0.48	0.53	0.48	0.51	0.48	0.52	0.52	0.56	0.52	0.46	0.47	0.57	0.47	0.55	0.58
Al_2O_3	12.68	12.35	12.08	12.28	12.14	12.66	12.10	11.54	12.15	12.26	11.99	11.51	12.28	11.74	11.98	12.20	12.19	11.97	12.00	12.01	11.14
Fe_2O_3	8.17	8.37	9.19	8.73	8.79	8.15	8.92	9.38	8.39	8.52	8.65	9.18	9.18	9.29	9.53	8.62	8.36	9.03	8.79	9.68	10.20
MnO	0.16	0.17	0.16	0.16	0.18	0.16	0.18	0.17	0.15	0.20	0.20	0.19	0.19	0.20	0.17	0.16	0.15	0.17	0.18	0.16	0.24
MgO	0.64	0.63	0.88	0.75	0.78	0.69	0.82	0.85	0.88	0.76	0.74	0.90	0.85	0.91	1.01	0.79	0.77	0.74	0.74	1.00	0.89
CaO	4.81	5.00	5.25	5.03	5.12	5.21	5.30	5.12	4.87	5.02	5.10	5.09	5.35	5.25	5.46	5.01	5.01	5.05	4.95	5.30	4.88
SrO	b.d.	0.06	b.d.	b.d.	0.05	0.06	b.d.	0.05	0.06	b.d.	b.d.	b.d.	b.d.	b.d.	b.d.	0.07	b.d.	b.d.	b.d.	0.06	b.d.
BaO	b.d.	b.d.	b.d.	b.d.	0.10	b.d.	0.07	b.d.	b.d.	b.d.	b.d.	b.d.	b.d.	b.d.	b.d.	b.d.	b.d.	b.d.	0.07	b.d.	b.d.
Na_2O	3.14	2.99	3.01	2.99	2.95	3.09	2.94	2.99	3.01	2.89	2.84	1.07	3.09	2.80	2.72	2.92	2.95	3.11	3.17	3.04	3.08
K_2O	0.77	0.79	0.69	0.75	0.72	0.78	0.76	0.67	0.72	0.72	0.72	0.72	0.68	0.69	0.68	0.74	0.69	0.71	0.74	0.71	1.12
P_2O_5	0.15	0.19	0.18	0.18	0.15	0.18	0.17	0.19	0.21	0.15	0.16	0.16	0.17	0.15	0.16	0.15	0.19	0.16	0.17	0.13	0.17
SO_3	0.05	b.d.	0.05	b.d.	0.03	0.07	0.05	0.06	b.d.	b.d.	b.d.	0.06	0.06	0.04	0.06	b.d.	b.d.	b.d.	0.03	0.04	0.05
F	b.d.	b.d.	b.d.	b.d.	0.03	b.d.	0.04	b.d.	b.d.	b.d.	0.04	0.03	b.d.	0.03	b.d.	b.d.	b.d.	b.d.	0.04	b.d.	0.04
Cl	0.22	0.23	0.23	0.25	0.22	0.26	0.25	0.27	0.22	0.24	0.24	0.27	0.26	0.27	0.24	0.22	0.24	0.24	0.22	0.25	0.26
TOTAL	100.19	99.47	99.75	99.81	99.26	100.11	99.18	99.64	99.93	99.17	99.03	99.17	99.59	99.92	99.91	99.91	99.64	100.44	100.27	100.30	100.45

SAMPLE	GS16-a18-1	GS16-a19-1	GS16-a19-1	GS16-a19-2	GS16-a19-3	SSR-1-11a	SSR-1-11b	SSR-1-11c	SSR-1-11d	SSR-1-11e	SSR-1-12	SSR-2-13a	SSR-2-13b	SSR-2-13c	SSR-2-13d	SSR-2-14a	SSR-2-14b	SSR-2-14c	SSR-2-14d	SSR-2-14e	SSR-4-15a
Sample Method	Grab Sample	Grab Sample	Grab Sample	Grab Sample	Grab Sample	Ocean surface	Ocean surface	Ocean surface	Ocean surface	Ocean surface	Ocean surface	Ocean surface	Ocean surface	Ocean surface	Ocean surface	Ocean surface	Ocean surface	Ocean surface	Ocean surface	Ocean surface	Ocean surface
Pumice Source	Seafloor	Seafloor	Seafloor	Seafloor	Seafloor	Raft	Raft	Raft	Raft	Raft	Raft	Raft	Raft	Raft	Raft	Raft	Raft	Raft	Raft	Raft	Raft
wt %																					
SiO_2	68.12	67.89	67.89	68.55	69.30	66.68	66.60	66.49	67.74	66.07	67.79	66.42	66.96	68.22	66.89	67.59	68.16	67.74	67.69	67.11	66.80
TiO_2	0.55	0.54	0.46	0.61	0.54	0.52	0.49	0.51	0.55	0.55	0.51	0.54	0.49	0.54	0.50	0.55	0.55	0.48	0.54	0.58	0.58
Al_2O_3	11.42	12.52	12.26	11.92	11.82	11.38	11.87	11.77	11.63	11.24	12.02	11.67	11.91	11.52	11.82	11.97	12.01	12.08	12.17	11.96	11.25
Fe_2O_3	9.39	8.39	8.76	8.92	8.50	9.18	9.24	9.11	9.30	9.74	9.00	9.04	9.00	8.94	9.26	8.55	8.63	8.75	8.60	8.75	9.80
MnO	0.14	0.13	0.15	0.20	0.14	0.18	0.18	0.19	0.18	0.23	0.15	0.15	0.16	0.16	0.21	0.15	0.20	0.20	0.17	0.17	0.19
MgO	0.71	0.72	0.67	0.75	0.71	1.02	0.96	0.97	1.09	1.15	1.00	0.96	0.98	1.08	1.08	0.96	0.93	0.92	0.88	0.94	1.04
CaO	5.06	5.19	4.98	4.75	4.60	5.31	5.22	5.32	5.20	5.42	5.38	5.30	5.40	5.07	5.46	5.26	5.23	5.19	5.23	5.27	5.42
SrO	b.d.	b.d.	0.07	b.d.	b.d.	0.06	0.02	0.05	0.02	0.04	0.03	0.06	b.d.	b.d.	0.04	b.d.	0.04	0.05	0.07	0.03	0.05
BaO	b.d.	0.09	0.09	b.d.	0.06	b.d.	b.d.	0.06	b.d.	b.d.	b.d.	b.d.	b.d.	0.06	0.07	0.07	b.d.	0.06	0.05	0.06	b.d.
Na_2O	3.19	3.12	3.01	3.00	3.09	2.85	2.95	2.97	2.75	2.68	2.99	3.01	2.98	2.71	2.94	2.82	3.07	2.99	3.02	2.96	2.80
K_2O	0.76	0.72	0.91	0.89	0.89	0.64	0.67	0.67	0.68	0.64	0.65	0.66	0.69	0.70	0.65	0.69	0.69	0.68	0.66	0.67	0.62
P_2O_5	0.14	0.14	0.15	0.18	0.16	0.14	0.16	0.15	0.16	0.18	0.14	0.20	0.15	0.17	0.19	0.15	0.17	0.18	0.16	0.16	0.15
SO_3	0.04	b.d.	b.d.	0.03	b.d.	0.07	0.09	0.07	0.04	0.09	b.d.	0.05	0.07	0.04	0.04	b.d.	b.d.	b.d.	0.03	b.d.	0.08
F	0.04	b.d.	b.d.	0.04	0.05	0.02	0.03	b.d.	0.01	0.03	0.02	b.d.	0.02	0.02	0.01	0.01	0.03	0.02	b.d.	0.02	b.d.
Cl	0.26	0.18	0.20	0.20	0.14	0.29	0.26	0.27	0.25	0.26	0.23	0.24	0.24	0.24	0.23	0.20	0.20	0.22	0.21	0.23	0.26
TOTAL	99.74	99.59	99.55	99.96	99.93	98.28	98.67	98.54	99.54	98.23	99.84	98.26	98.98	99.40	99.31	98.91	99.85	99.51	99.45	98.85	98.97

SAMPLE	SSR-4-15b	SSR-4-15c	SSR-4-15d	SSR-4-16a	SSR-4-16b	SSR-4-16c	SSR-5-17a	SSR-5-17b	SSR-5-17c	SSR-5-17d	SSR-5-18a	SSR-5-18b	SSR-5-18c	SSR-5-18d	SSR-5-18e	SSR-7-19	SSR-7-20a	SSR-7-20b	SSR-7-20c	SSR-7-20d
Sample Method	Ocean surface	Ocean surface	Ocean surface	Ocean surface	Ocean surface	Ocean surface	Ocean surface	Ocean surface	Ocean surface	Ocean surface	Ocean surface	Ocean surface	Ocean surface	Ocean surface	Ocean surface	Ocean surface	Ocean surface	Ocean surface	Ocean surface	Ocean surface
Pumice Source	Raft	Raft	Raft	Raft	Raft	Raft	Raft	Raft	Raft	Raft	Raft	Raft	Raft	Raft	Raft	Raft	Raft	Raft	Raft	Raft
wt %																				
SiO_2	66.80	67.07	67.77	67.87	67.31	67.43	67.60	67.18	67.35	67.76	67.79	68.28	68.15	68.36	67.63	67.71	69.05	67.39	68.02	67.45
TiO_2	0.55	0.52	0.58	0.51	0.49	0.52	0.53	0.50	0.56	0.52	0.48	0.51	0.55	0.58	0.52	0.54	0.54	0.53	0.52	0.55
Al_2O_3	11.39	11.41	11.68	12.09	11.98	11.92	11.25	11.95	11.83	12.09	11.92	11.74	12.03	11.82	11.96	11.90	12.08	11.92	11.93	11.97
Fe_2O_3	9.51	9.60	8.40	9.02	8.89	9.12	9.34	8.92	8.69	8.67	8.78	8.70	8.87	8.87	8.73	9.07	8.99	8.87	8.98	8.61
MnO	0.18	0.16	0.14	0.17	0.17	0.18	0.19	0.22	0.20	0.14	0.18	0.18	0.21	0.15	0.18	0.20	0.16	0.17	0.16	0.17
MgO	1.14	1.05	1.04	0.88	0.94	0.97	0.99	0.82	0.77	0.87	0.98	0.92	0.94	0.92	0.89	0.88	0.99	0.87	1.00	0.94
CaO	5.48	5.42	5.02	5.25	5.41	5.33	5.27	5.22	5.14	5.02	5.22	5.07	5.32	5.28	5.20	5.31	5.46	5.30	5.42	5.29
SrO	b.d.	0.07	0.04	b.d.	0.02	0.03	0.07	0.03	0.03	b.d.	0.04	0.09	0.02	0.02	0.06	0.04	0.03	0.07	0.04	0.05
BaO	b.d.	0.06	0.06	0.08	b.d.	b.d.	0.05	0.06	b.d.	b.d.	0.08	b.d.	0.07	b.d.	0.07	b.d.	0.05	b.d.	b.d.	0.05
Na_2O	2.71	2.86	3.23	3.03	2.90	2.93	2.94	3.09	3.02	2.99	2.78	2.88	2.98	3.04	2.92	2.87	0.29	2.84	2.85	2.90
K_2O	0.65	0.64	0.72	0.66	0.67	0.68	0.67	0.68	0.70	0.69	0.66	0.68	0.69	0.73	0.67	0.67	0.68	0.70	0.68	0.66
P_2O_5	0.19	0.16	0.15	0.17	0.13	0.15	0.15	0.17	0.16	0.18	0.14	0.18	0.14	0.17	0.18	0.14	0.15	0.16	0.16	0.15
SO_3	0.08	0.08	0.03	0.03	b.d.	0.06	0.08	0.04	0.06	0.07	0.05	0.05	b.d.	0.04	b.d.	0.03	b.d.	b.d.	0.03	b.d.
F	0.02	0.03	0.03	b.d.	0.01	0.02	b.d.	b.d.	0.02	b.d.	b.d.	0.04	0.01	0.02	0.02	b.d.	0.04	b.d.	0.01	0.01
Cl	0.26	0.26	0.22	0.25	0.24	0.23	0.27	0.26	0.24	0.26	0.22	0.25	0.24	0.23	0.23	0.24	0.20	0.24	0.20	0.23
TOTAL	98.89	99.32	99.05	99.95	99.10	99.53	99.34	99.07	98.71	99.20	99.25	99.51	100.14	100.18	99.18	99.54	98.66	99.00	99.96	98.99

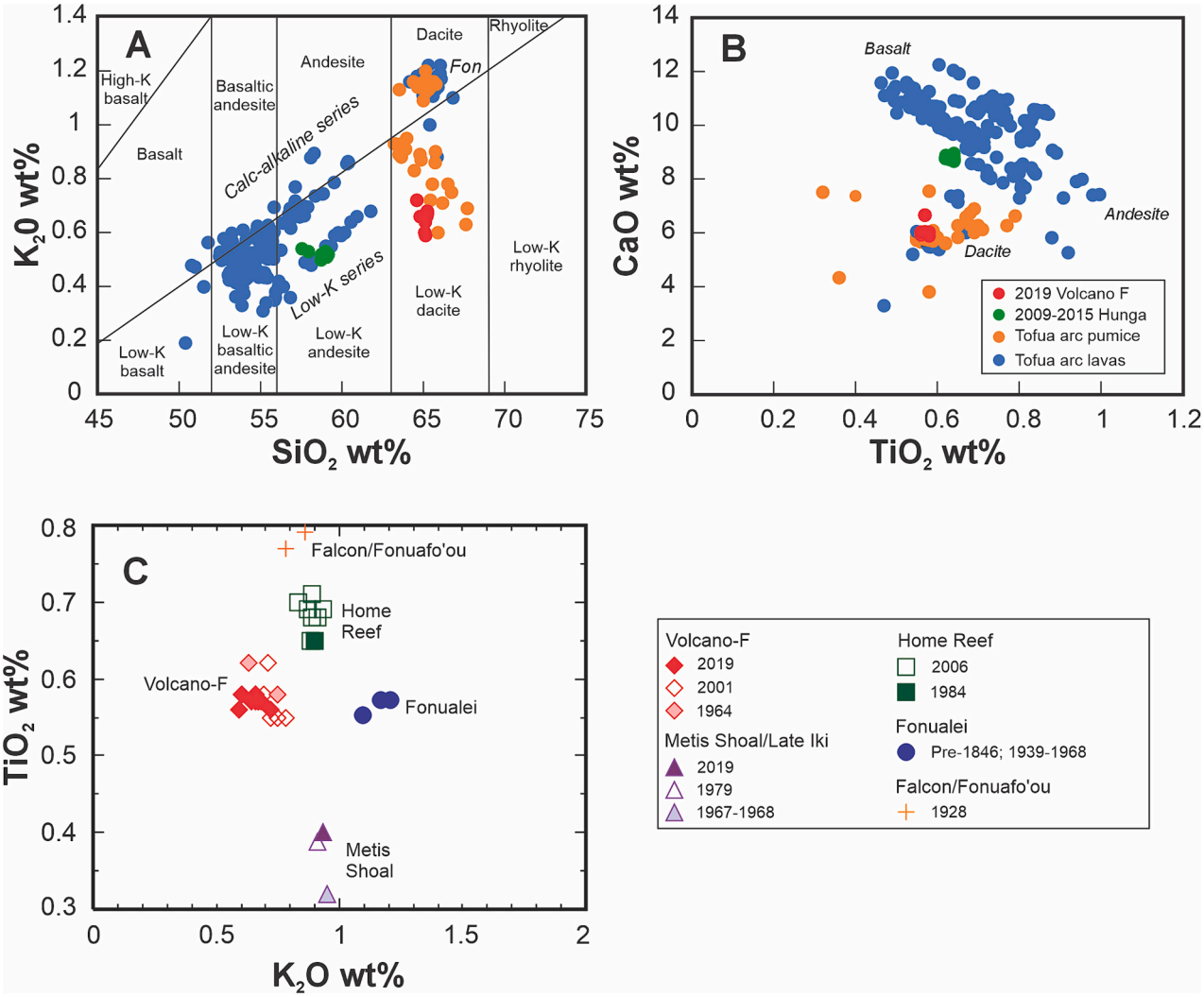

Fig. 7. Major element compositional characteristics of the 2019 eruption from Volcano-F in relation to other eruptive products from the Tofua Arc. A) K_2O-SiO_2 classification diagram of Ewart (1982) illustrating the low-K dacite composition of pumice raft-forming eruptions over the last 100 years, which contrast with dacite lavas and associated pyroclastic cones from Fonualei (Fon) that are calc-alkalic (Turner et al., 2012; Beier et al., 2017). Mafic lavas in the Tofua Arc are dominantly basaltic andesite in composition with andesite being rare. Andesite is more prevalent at Hunga Volcano where the recent eruptive activity that began in 2009 is low-silica andesite (Reagan et al., 2017). B) CaO vs TiO_2 plot showing the Tofua pumice rafts lie off trend and likely have a different petrogenesis to lavas within the Tofua Arc. C) TiO_2-K_2O plot that discriminates dacite pumice compositions from different volcanoes and highlights the close chemical similarity for multiple eruptions from the same volcano. The pumice described by Ewart et al. (1998) following an apparent eruption in 1964 shows a very close compositional similarity to pumice erupted from Volcano-F in 2001 and 2019. Data sources: Falcon/Founuafo'ou (Lacroix, 1939, 1940); Fonualei (Melson et al., 1970; Bryan et al., 1972; Ewart et al., 1973; Turner et al., 2012; Beier et al., 2017; Reagan et al., 2017); Home Reef (Bryan unpublished data; Reagan et al., 2017); Metis Shoal/Late'iki (Melson et al., 1970; Ewart et al., 1973; Turner and Hawkesworth, 1997; this study); Volcano-F (Bryan, 1968; Bryan et al., 2004; this study).

4. Discussion

4.1. Was the 2019 eruption of Volcano-F explosive?

Due to the remote, underwater locations and their short-lived nature, direct observations of the relatively frequent pumice raft-producing eruptions from the Tofua arc have been sparse. The 2019 eruption of Volcano-F was no exception and the main phase of the eruption occurred at a time of extensive cloud cover, preventing capture in images from the readily accessible satellites such as MODIS Terra and Aqua, Sentinel-3, and Suomi-VIIRS, which pass sequentially over the same area within a few hours each day. Unobscured images show two concentric rings in the water on the 7th August 2019 and discoloured water in the vicinity of the volcano and drifting away from it on the 9th and 11th August (Brandl et al., 2020; Jutzeler et al., 2020). A single eyewitness report made by an employee of Hukula Lodge on Vava'u confirmed the 2019 eruption of Volcano-F broke the sea surface at some point around the 7th August, but while they describe low level steam-rich plumes and explosions in the vicinity of the volcano, they were unable to be more specific. Volcano F also lies to the north of inhabited Tongan islands, and away from typical flight paths, limiting the potential for other eyewitness accounts. There were two earthquakes detected in the vicinity of Volcano-F around the time of the eruption; 4.5 M_w at 10:56:22 and 4.2 M_w at 14:10:15, supporting an eruption duration of less than a day. While other smaller earthquakes may have occurred, they would not have been detected because of the poor seismic coverage. Sub-Plinian eruptions lasting several hours are common for volcanoes in this region and typically produce steam-rich plumes that reach a few kilometres in height. Although a sub-Plinian plume was not observed for Volcano-F, it is possible that one was produced and dispersed between satellite images and avoided direct observation because of the lack of boats or aircraft in this airspace.

Satellite-detected SO_2 plumes are a valuable indicator of sustained explosive eruptions (e.g. Carn et al., 2017). There is no associated SO_2

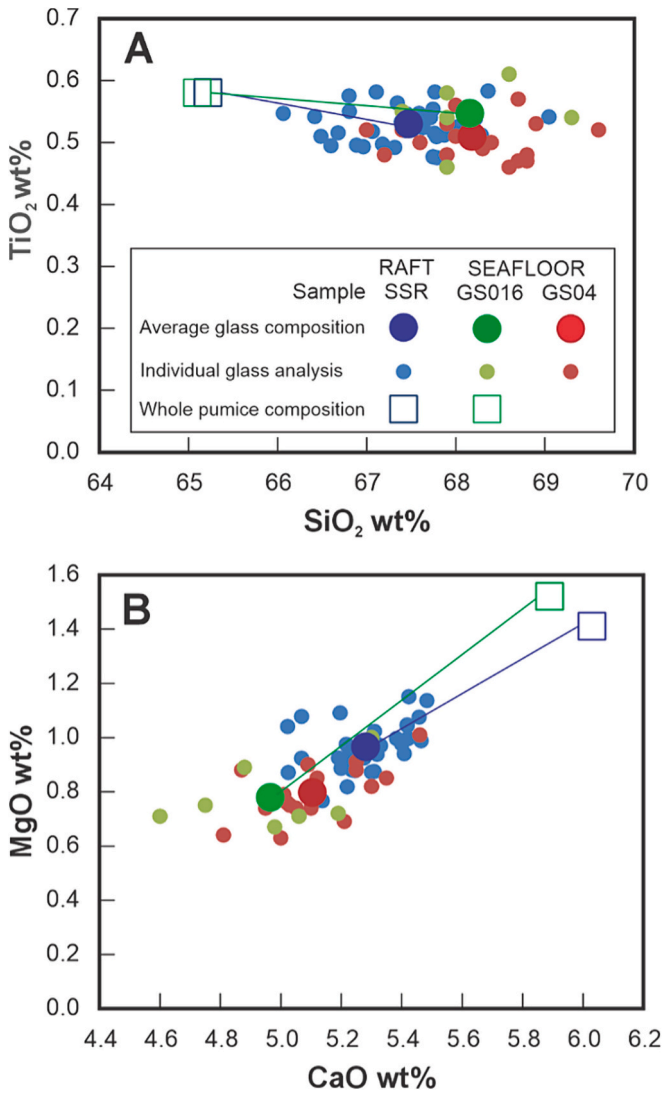

Fig. 8. Binary plots comparing pumice glass and whole pumice compositions from the 2019 eruption of Volcano-F. A) Harker diagram showing TiO2 variation with SiO2. Tie lines connect whole-pumice compositions (determined by XRF) with average glass compositions (determined by electron microprobe analysis). Pumice glass compositions are more silicic than whole-pumice compositions, and seafloor pumice are slightly more silicic than raft pumice. B) MgO vs CaO binary plot showing pumice glass compositions are more depleted in MgO and CaO than whole-pumice compositions, and that raft pumice glass has slightly higher MgO and CaO contents than associated seafloor pumice glass. In both plots, whole-pumice data are normalised to 100% on an LOI-free basis and the pumice glass compositions are normalised to 100%.

plume captured by Sentinel 5 on the 6th, 7th, 8th or 9th of August, suggesting large, sustained, high eruption plumes were not generated. This is not unusual for lower VEI eruptions in this region. Since the region has been covered by the Sentinel-5 satellite (since 2018) there have been five eruptions reported from volcanoes in the region, Volcano-F in 2019, Late'iki in 2019 (Yeo et al., 2022), Hunga Volcano in 2021/22 (Gupta et al., 2022; Lynett et al., 2022; Borrero et al., 2023; Le Mével et al., 2023; Seabrook et al., 2023; Clare et al., 2023) and two eruptions of Home Reef in 2022 and 2023. The 2022 and 2023 eruptions of Home Reef and the 2019 eruption of Late'iki did not produce a detectable SO_2 plume. In contrast, even the early phases of the Hunga Volcano eruption generated a clear SO_2 anomaly.

We suggest that given the vent depth, and comparison to other eruptions in the region, the eruption of Volcano-F likely broke the ocean surface, with one or more sub-Plinian explosive phases lasting only a few hours, similar to the reports of the 2001 eruption. The pumice raft was likely produced by explosive phases, although submarine contributions cannot be ruled out. This highlights the difficulty with understanding volcanic processes at poorly observed volcanoes, where sparse satellite observations may not capture all the phases of the eruption.

4.2. *Vent location and reorganisation following the 2019 eruption*

Bathymetric changes determined from the 2020 post-eruption seafloor survey indicate that the eruption was sourced from the northern section of the caldera rim, and that there was a slight westward shift in the location of the vent from the 2001 eruption. The new crater, sitting 200 m NW of the nearest pre-existing structure, has a diameter of 80 m and a depth of 45 m, being slightly smaller than the three pre-existing craters imaged in the same area (Fig. 3) by Brandl et al. (2020), with diameters of 250 m, 145 m and 230 m (the active crater during the 2001 eruption). This region on the caldera rim appears to be the focus of the most recent volcanic activity and lies at the intersection of two regions of pumice cones, one that follows the caldera rim and a second that forms a roughly NE-SW ridge across the caldera floor (Fig. 1). The 2019 eruption occurred at the NW end of this alignment. The northwest-trending chain of craters is located on the shallowest section of the submarine caldera complex, where the caldera rim rises from caldera floor depths of 670–720 m to 30 m below sea level. Silicic lavas/domes form the upper parts of the shallow northern caldera rim recording an earlier period of effusive and constructional volcanism. Recent explosive eruptions now blanket the lavas in layers of loose pyroclastic material (Fig. 5). In water depths of 30–60 m, the pyroclastic material appears to have been remobilised, probably by wave action forming ripple-scale symmetrical bedforms composed of pumice (Fig. 5).

Clast distributions are complicated by later reworking, but clast size data (Fig. 6) show a trend for larger median and maximum clast sizes towards the west and towards craters. Very large pumice clasts (diameters >1 m) were observed only within or directly next to the new vent, but pumice clasts with diameters up to 30 cm were found >600 m away from the summit, suggesting substantial transport of large material during the eruption, possibly at the sea surface. The entire summit is covered by small pumice (< 5 cm), but this is also the material most likely to be quickly remobilised and moved by current and wave action, may be generated by wave action on the substrate and may not all derive from the 2019 eruption.

The absence of sessile fauna and the presence of some active or recent hydrothermal fluid venting, as indicated by alteration on samples and biofilms imaged by the ROV and equipment cameras (Fig. 2), support the observations that the new, westernmost crater was active during the 2019 eruption. It also appears that major disturbance to the benthic communities in the region was mostly limited to the area within 600–1000 m of the eruption, although the impacts down-current may have extended further. This crater also aligns well with the location of the eruption plume (Fig. 1B). We cannot completely rule out other nearby craters being active during the 2019 eruption but there is no evidence from the satellite data or from seafloor observations. Bacterial mats in the crater just east of the newly formed one suggest fluid flow in this region. Assuming a single vent was active and that its diameter was not substantially modified during or after the eruption, the maximum conduit diameter was <100 m, which appears typical for recent eruptions at Volcano-F given the similar diameters of other craters.

The distribution of seafloor hydrothermal alteration appears to be primarily proximal to the active vent, with no evidence of hydrothermal fluid venting from anywhere else on the summit. Only very minor temperature deviations are noted, suggesting no anomalously high-temperature fluid flow from this region six months after the eruption. The eruption was not preceded by any water discolouration observable from satellites and discoloured water was only observed during the period of the eruption, unlike the previous 2001 eruption where water discolouration was observed two weeks after the eruption finished.

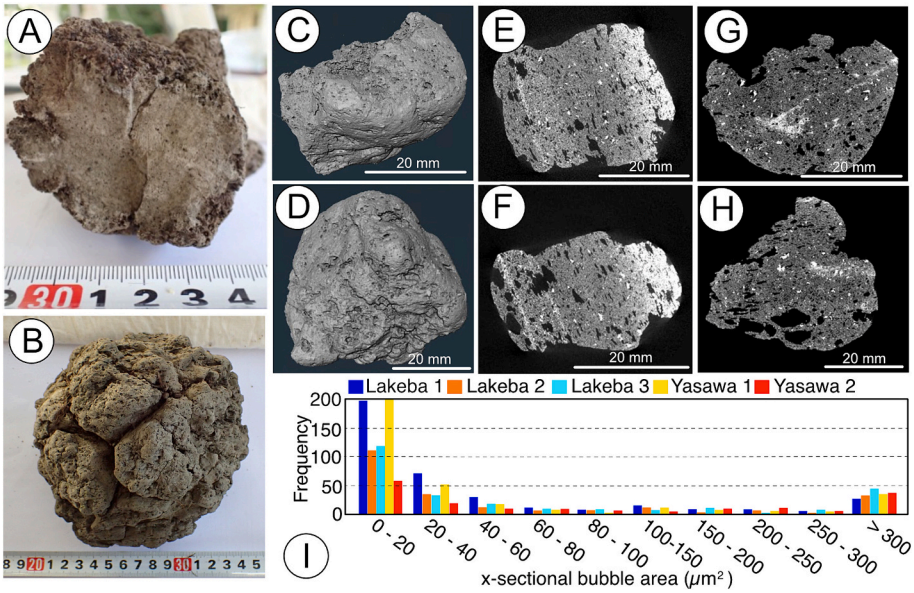

Fig. 9. Samples collected during fieldwork and pumice characteristics from XRCT data. A & B) Field photographs (ruler divisions in cm) of samples collected on Lakeba (A) and Yasawa (B) showing breadcrust textures; C&D) Reconstructed clast shapes from raft samples scanned by XRCT characteristic of smooth raft material; *E*-H) Orthoslices through pumices scanned using XRCT from Lakeba (D, E, F) and Yasawa (C, G, H). The brightly reflective edges on E and F are the chilled bark-like textures observed on some samples, other brighter regions represent different densities not due to cooling; I) Cross-sectional areas for pumice clasts analysed across 5 scans for samples from Lakeba and Yasawa.

4.3. The 2019 eruption of Volcano-F was a VEI 3 eruption

Brandl et al. (2020) estimated a DRE raft volume of between $2.5*10^6$ m^3 and $12.3*10^6$ m^3. From our mapping we find an additional $3.1*10^7$ m^3 bulk volume of material was added, with a DRE of around 5.6 $*10^6$ m^3, resulting in a minimum total eruption volume of between 8.1 $*10^6$ m^3 and $17.9*10^6$ m^3 (i.e. 0.02–0.03 km^3), equivalent to a volcanic explosivity index (VEI) of 3. This is at the highest end of the VEI 2–3 calculated by Brandl et al. (2020) that was based on raft volume alone. Our study does not map out the entire region of seafloor affected by the eruption and thus some seafloor material is likely not captured and our DRE calculation is thus a minimum estimate. However, even if the seafloor component was doubled, the DRE eruption volume would still be categorised as a VEI 3, making this the most likely VEI category and consistent with eyewitness accounts. This highlights the difficulty with applying VEI scales to submarine eruptions, even those which produce a pumice raft, because not all of the material is partitioned into the raft and some will form submarine deposits. Ignoring submarine deposits can therefore result in a underestimate of the VEI. VEI estimation is complicated by the fact that different eruptions may partition more or less material as a percentage into the raft. When Havre (Jutzeler et al., 2014; Carey et al., 2018; Manga et al., 2018a; Mitchell et al., 2018, 2021) erupted in 2012 > 90% of material entered the raft. However, depending on the raft volume used, at Volcano F between 30% and 70% entered the raft and remained in it long enough to be imaged, meaning a substantial proportion of the material accumulated at the vent and down current. This shows that there may be considerable variability between volcanoes and eruptions and that VEI cannot be confidently attributed from pumice raft volume alone.

4.4. A consistent source for at least three eruptions of Volcano-F within the last 60 years

Geochemical analyses performed on pumice collected from the seafloor show they are similar to pumice from the raft (Table 1). No chemical difference is observed either in raft material collected within days of the eruption (sample SSR, Table 1), from Fiji, arriving ~6 weeks after eruption, or pumice that eventually washed up in eastern Australia (sample Gold Coast 1, Table 1). We therefore conclude that the eruption was derived from a homogenous batch of dacitic magma.

The pumice rafts from Volcano-F are slightly more silicic than dredged samples from seafloor lavas from Volcano-F (Brandl et al., 2020), indicating that the most silicic magma compositions erupt explosively. The 2019 pumice compositions are remarkably similar to the 2001 pumice (Global Volcanism Program, Smithsonian Institution, 2003) with overlapping abundances for some elements (K_2O, MgO, MnO, TiO_2) but subtle differences for others (SiO_2, Fe_2O_3T, Y, Zr, Zn, Cu). The non-systematic element differences and slightly lower SiO_2 content rule out the 2019 magma as being produced by closed system fractionation of the 2001 parental composition. The subtly higher abundances of CaO, MgO, Fe_2O_3T and some chalcophile and siderophile elements of Cu, Zn, Cr and Co suggest some diffuse contributions such as by gas sparging from a more mafic magma, and some basaltic recharge at depth may have been a trigger for the 2019 eruption. Mafic recharge could promote the mingling type textures observed in the XRCT scans of the pumice clasts (Fig. 9); however, further geochemical analysis is required to understand if this is the case. Although only major element data are available, a close similarity also exists between the 2001 and 2019 pumice compositions and pumice collected in 1964 from the Coral Sea islands following an unobserved eruption (Bryan, 1968). The geochemical distinction of erupted materials from other volcanoes in the Tofua arc (Fig. 6) indicates that the 1964 eruption was also from Volcano-F. We therefore infer that Volcano-F has had at least three explosive eruptive episodes in the last 60 years.

4.5. The similarities and differences between Volcano-F, other active Tofua-Arc calderas, and the significance of smaller VEI eruptions

Volcano-F is one of at least 10 caldera volcanoes along 750 km of the Tofua Arc north of 22°S (Table 3), some of which have previously been misclassified as stratovolcanoes (Global Volcanism Program, Smithsonian Institution) and 6 of which remain unnamed. Continued future mapping of the region may reveal additional calderas that are not currently known and are also active, for example no high-resolution bathymetry is currently available of the very active Home Reef volcano. These calderas are not all the same, they have variable

Table 3
Names, locations, eruptive histories and morphology of submerged calderas north of 22°S on the Tofua Arc. Data is extracted from the Smithsonian database where available (Global Volcanism Program, Smithsonian Institution) or measured from compiled bathymetry of the Tofua Arc (Ryan et al., 2009), RV Southern Surveyor cruise SS2004/11 and RV Sonne cruise SO-267 (Hannington et al., 2019).

Volcano	Latitude	Longitude	Eruption History	Primary lava type	Caldera floor depth (mbsl)	Shallowest depth	Depth resurgent cones/ domes	Caldera dimensions	Pumice raft forming?	Other
Curacoa	−15.62	−173.67	1973 (VEI 3), 1979 (VEI 1)	Dacite	830	68	68	13 × 8 km	Yes	
Unnamed	−16.54	−173.76	Unknown	Unknown	668	159	300	5.5 x collapsed	Unknown	Appears to have suffered a major collapse
Volcano-F	−18.33	−174.37	2001 (VEI 2), 2019 (VEI 3)	Dacite	725–440	40	40	7.5 × 5 km	Yes	
Unnamed	−19.42	−174.93	Unknown	Unknown	970	307	411	5.5 × 5.5 km	Unknown	
Tofua	−19.75	−175.07	1774 (VEI 2), 1792 (VEI 0), 1845, 1847 (VEI 1), 1854 (VEI 2), 1885 (VEI 2), 1906 (VEI 2) 1906 (VEI 2) 1958 (VEI 2) 2004 (VEI 1) 2015 - present (VEI 0)	Basaltic andesite, dacite	500	Suaerial	Subaerial	5 × 5 km	No	
Unnamed	−20.12	−175.17	Unknown	Unknown	849	407	576	10 × 6 km	Unknown	
Hunga Volcano	−20.55	−175.38	1912 (VEI 2), 1937 (VEI 2), 1988 (VEI 0), 2009 (VEI 2), 2014 (VEI 3), 2021/2022 (VEI 5–6)	Basaltic andesite, andesite	800	Subaerial	None following 2022 eruption	4.5 × 4.5 km	Yes	
Unnamed	−21.15	−175.74	Unknown	Unknown	470	121	121	5.5 × 4 km	Unknown	
Unnamed	−21.3	−179.65	Unknown	Unknown	545	206	206	6 × 4 km	Unknown	
Unnamed	−21.8	−175.94	Unknown	Unknown	862	51	223	5 × 5 km	Unknown	Activity moved to new vent site NNW of caldera

geochemistry and eruptive histories; however, there are also similarities. They have similar dimensions, caldera floor depths, and many have shallow resurgent vent sites on their caldera rims, which are the sites of most recent, <VEI 4 eruptions. All of them have shallow vents, where the overlying water column would not meaningfully supress an explosive eruption. While records are incomplete for their eruptive histories, four of these calderas seems to be erupting regularly and recently: Curacoa, Volcano-F, Tofua and Hunga Volcano. Except for Hunga Volcano (discussed below), there is no evidence that any of these calderas produced recent large caldera forming eruptions, thus all may be in the recharge phase of their caldera cycles and, as highlighted by recent evidence from Santorini caldera (Preine et al., 2024), may pose the risk of a large eruption at any time. While other volcanoes are more geochemically similar to Volcano-F in the Tofua Arc, in this section we focus on those that have a caldera morphology that suggests they are capable of large volume explosive eruptions.

The large VEI 5 eruption in 2021/2022 of Hunga Volcano eruption was preceded by multiple VEI 3 or lower eruptions, in 1988, 2009 and 2014/15 (Brenna et al., 2022), none of which showed any obvious priming of the caldera for such an explosive event. While the mechanism for the explosivity of this eruption is still debated (Cronin et al., 2023; Henley et al., 2024) and a discussion of these mechanisms is beyond the scope of this study, the major explosive event was preceded by weeks of volcanic activity at the site, which became progressively more explosive on 14th January 2022, and the major explosive event was accompanied by a change in the geochemistry of erupted products (Cronin et al., 2023). This suggests some reorganisation of the magma plumbing system beneath the volcano between these eruption phases, as supported by gravity data (Le Mével et al., 2023), possibly as a result of activity on 14th January 2022. While Volcano-F is geochemically distinct from Hunga Volcano, it is regularly erupting batches of geochemically similar but distinct magmas from a caldera rim vent site, which show some evidence of magma mixing. Repeated eruptions of similar composition and low crystal content magma over decadal to centennial scales suggests existence of a melt-dominant magma body beneath the volcano. In the traditional caldera cycle this would be consistent with a volcano in either the post-collapse or recharge phase (Cole et al., 2005), while in the revised model (de Maisonneuve et al., 2021) the eruption of magmatic products distinct from those that formed the whole caldera would indicate the onset of a new caldera cycle. Therefore, while not completely the same as Hunga volcano, conditions exist at Volcano-F to suggest it is capable of much more explosive eruptions than it has produced over the last few decades. Smaller eruptions at this volcano, and others in the Arc, should be carefully monitored and properly characterised, both because they have the potential to trigger more explosive eruptions, and because they provide geochemical evidence on the plumbing system of the volcano, particularly when properly documented over decades.

5. Conclusions

Based on data acquired rapidly after the 2019 eruption of Volcano-F, we conclude that the eruption was a VEI 3 sub-Plinian eruption, likely lasting less than a day. New geochemical analyses on sampled products from the 2019 eruption, including whole pumice compositions and glass chemistry, confirm the erupted magma composition was dacitic. The low-K dacite composition is consistent with the composition of other historic pumice raft-forming eruptions from the Tofua arc. The 2019 pumice compositions are remarkably consistent between seafloor and raft deposits suggesting a homogenous batch of dacite was erupted. Very subtle differences in some elements are observed between the 2001 and 2019 pumice compositions but slightly lower SiO2, and higher CaO, Fe_2O_3, and Al_2O_3 argue against the 2019 dacite being simply produced by fractionation of a 2001 parental dacite magma composition and, along with textural evidence, support more complex plumbing beneath the caldera.

New surveys following the 2019 eruption confirm the shallow water depths for vents that erupted in 2001 and 2019 and that the eruption generated a new crater near the site of the 2001 eruption crater. The volcano is shoaling with summit depths now within 40 m of sea level. A

series of craters are identified in bathymetric datasets ranging between ~145 and 250 m in diameter with crater depths of up to ~45 m beneath the crater rim. Here, the shallow water depth for the vent did not limit eruption explosivity and a sub-Plinian-type eruption is interpreted to have produced the pumice raft, consistent with observations of earlier pumice raft-producing eruptions in the Tofua Arc.

The eruption frequency over the last few decades suggests that Volcano-F, and other calderas in this region, may be at various stages of recharge, and therefore pose a risk of major volcanic eruptions. Hazardous calderas in the region will have shallow vent depths, decadal or more frequent eruptions (which may or may not show geochemical variability) and multiple magma reservoirs. Volcanic histories are incomplete and the region has almost no monitoring aside from satellite data. These active caldera volcanoes should be targets for further study and monitoring in the future.

Supplementary data to this article can be found online at https://doi.org/10.1016/j.jvolgeores.2024.108160.

CRediT authorship contribution statement

Isobel A. Yeo: Writing – original draft, Resources, Project administration, Investigation, Funding acquisition, Formal analysis, Data curation, Conceptualization. **Iona M. McIntosh:** Writing – review & editing, Resources, Project administration, Investigation, Funding acquisition, Formal analysis, Data curation, Conceptualization. **Scott E. Bryan:** Writing – review & editing, Writing – original draft, Investigation, Funding acquisition, Formal analysis, Conceptualization. **Kenichiro Tani:** Writing – review & editing, Writing – original draft, Investigation, Formal analysis, Data curation. **Matthew Dunbabin:** Writing – review & editing, Methodology, Investigation, Formal analysis. **Katherine J. Dobson:** Writing – review & editing, Formal analysis. **Samuel J. Mitchell:** Writing – review & editing, Formal analysis. **Patrick C. Collins:** Writing – review & editing, Project administration, Investigation. **Michael A. Clare:** Writing – review & editing, Formal analysis. **Henrietta Cathey:** Formal analysis. **Isikeli Duwai:** Methodology, Investigation. **Philipp A. Brandl:** Writing – review & editing, Formal analysis. **Karen Stone:** Methodology, Investigation. **Mele S. Manu:** Methodology, Investigation.

Declaration of competing interest

The authors declare the following financial interests/personal relationships which may be considered as potential competing interests.

Isobel Yeo reports financial support was provided by National Oceanography Centre. If there are other authors, they declare that they have no known competing financial interests or personal relationships that could have appeared to influence the work reported in this paper.

Data availability

All geochemical data is available with the manuscript. Bathymetric data will be available through BODC on publication.

Acknowledgements

We thank Dr. Marco Brenna and an anonymous reviewer for their careful and detailed reviews, which have greatly improved this manuscript. We thank Kirsty Bowe, Allan Bowe, Pook Twomey and Nusa for invaluable assistance with the survey work, and their accounts of the history of eruptions in this region, which have helped to contextualise this work. Authors thank the Vava'u Environmental Protection Association for assistance in the field and with logistics. We are grateful to Alistair Grinham for assistance with bathymetry processing. Thanks also to Mark Hannington for useful discussion and for permission to reproduce bathymetry in this submission. Further thanks to Michael and Larissa Brill for providing us with samples of the pumice raft. We are grateful to the Ministry of Lands and Resources, Kingdom of Tonga and the Fiji Ministry of Lands & Mineral Resources for granting permission to undertake the surveys and sample collection. This research was supported by NERC is the Natural Environmental Research Council Urgency Grant NE/T010916/1.

References

Allen, S.R., Fiske, R.S., Cashman, K.V., 2008. Quenching of steam-charged pumice: Implications for submarine pyroclastic volcanism. Earth Planet. Sci. Lett. 274, 40–49. https://doi.org/10.1016/j.epsl.2008.06.050.

Arculus, R.J., SS2004/11 shipboard scientists, 2004. S11/2004 Voyage Summary: NoToVE-2004 (Northern Tonga Vents Expedition): Submarine Hydrothermal Plume Activity and Petrology of the Northern Tofua Arc, Tonga.

Beier, C., Turner, S.P., Haase, K.M., Pearce, J.A., Münker, C., Regelous, M., 2017. Trace element and isotope geochemistry of the northern and central Tongan islands with an emphasis on the genesis of high Nb/Ta signatures at the northern volcanoes of Tafahi and Niuatoputapu. J. Petrol. 58, 1073–1106.

Bohnenstiehl, D.R., Dziak, R.P., Matsumoto, H., Lau, T.-K.A., 2013. Underwater acoustic records from the March 2009 eruption of Hunga Ha'apai-Hunga Tonga volcano in the Kingdom of Tonga. J. Volcanol. Geotherm. Res. 249, 12–24.

Borrero, J.C., et al., 2023. Tsunami Runup and Inundation in Tonga from the January 2022. Erupt. Hunga Volcano: Pure Appl. Geophys. 180, 1–22. https://doi.org/10.1007/s00024-022-03215-5.

Brandl, P.A., Schmid, F., Augustin, N., Grevemeyer, I., Arculus, R.J., Devey, C.W., Petersen, S., Stewart, M., Kopp, H., Hannington, M.D., 2020. The 6–8 Aug 2019 eruption of 'Volcano F' in the Tofua Arc, Tonga. J. Volcanol. Geotherm. Res. 390, 106695 https://doi.org/10.1016/j.jvolgeores.2019.106695.

Brenna, M., Cronin, S.J., Smith, I.E.M., Pontesilli, A., Tost, M., Barker, S., Tonga'onevai, S., Kula, T., Vaiomounga, R., 2022. Post-caldera volcanism reveals shallow priming of an intra-ocean arc andesitic caldera: Hunga volcano, Tonga, SW Pacific. Lithos 412, 106614.

Bryan, W.B., 1968. Low-potash dacite drift pumice from the Coral Sea. Geol. Mag. 105, 431–439.

Bryan, W.B., Stice, G.D., Ewart, A., 1972. Geology, petrography, and geochemistry of the volcanic islands of Tonga. J. Geophys. Res. 77, 1566–1585.

Bryan, S.E., Cook, A., Evans, J.P., Colls, P.W., Wells, M.G., Lawrence, M.G., Jell, J.S., Greig, A., Leslie, R., 2004. Pumice rafting and faunal dispersion during 2001–2002 in the Southwest Pacific: record of a dacitic submarine explosive eruption from Tonga. Earth Planet. Sci. Lett. 227, 135–154. https://doi.org/10.1016/j.epsl.2004.08.009.

Bryan, S.E., Cook, A.G., Evans, J.P., Hebden, K., Hurrey, L., Colls, P., Jell, J.S., Weatherley, D., Firn, J., 2012. Rapid, long-distance dispersal by pumice rafting. PLoS One 7, e40583. https://doi.org/10.1371/journal.pone.0040583.

Carey, S., Sigurdsson, H., Mandeville, C., Bronto, S., 1996. Pyroclastic flows and surges over water: an example from the 1883 Krakatau eruption. Bull. Volcanol. 57, 493–511. https://doi.org/10.1007/BF00304435.

Carey, R., et al., 2018. The largest deep-ocean silicic volcanic eruption of the past century. Sci. Adv. 4, 1–7. https://doi.org/10.1126/sciadv.1701121.

Carn, S., Fioletov, V., McLinden, C., Li, C., Krotkov, N., 2017. A decade of global volcanic SO2 emissions measured from space. Sci. Rep. 7, 44095.

Carvajal, M., Sepúlveda, I., Gubler, A., Garreaud, R., 2022. Worldwide signature of the 2022 Tonga volcanic tsunami. Geophys. Res. Lett. 49 e2022GL098153.

Casalbore, D., Clare, M.A., Pope, E.L., Quartau, R., Bosman, A., Chiocci, F.L., Romagnoli, C., Santos, R., 2021. Bedforms on the submarine flanks of insular volcanoes: New insights gained from high resolution seafloor surveys. Sedimentology 68, 1400–1438.

Clare, M.A., et al., 2023. Fast and destructive density currents created by ocean-entering volcanic eruptions. Science 381, 1085–1092. https://doi.org/10.1126/science.adi3038.

Cole, J., Milner, D., Spinks, K., 2005. Calderas and caldera structures: a review. Earth Sci. Rev. 69, 1–26.

Colombier, M., Scheu, B., Wadsworth, F.B., Cronin, S., Vasseur, J., Dobson, K.J., Hess, K., Tost, M., Yilmaz, T.I., Cimarelli, C., 2018. Vesiculation and Quenching during Surtseyan Eruptions at Hunga Tonga-Hunga Ha'apai Volcano, Tonga. J. Geophys. Res. Solid Earth 123, 3762–3779.

Cronin, S.J., Paredes-Mariño, J., Ukstins, I., Wu, J., Hamilton, K., Adams, D., Colombier, M., Huebsch, M., White, J.D., Brenna, M., 2023. Is the 2022 Hunga Event a New Phreatomagmatic Eruption Type? AGU23.

de Maisonneuve, C.B., Forni, F., Bachmann, O., 2021. Magma reservoir evolution during the build up to and recovery from caldera-forming eruptions–a generalizable model? Earth Sci. Rev. 218, 103684.

ESA. https://apps.sentinel-hub.com/eo-browser/?zoom=14&lat=-18.30495&lng=-174.40654&themeId=DEFAULT-THEME&visualizationUrl=https%3A%2F%2Fservices.sentinel-hub.com%2Fogc%2Fwms%2F42924c6c-257a-4d04-9b8e-36387513a99c&datasetId=S2L1C&fromTime=2019-08-06T00%3A00%3A00.000Z&toTime=2019-08-06T23%3A59%3A59.999Z&layerId=1_TRUE_COLOR&demSource3D=%22MAPZEN%22, 2019.

Ewart, A., Bryan, W.B., Gill, J.B., 1973. Mineralogy and Geochemistry of the Younger Volcanic Islands of Tonga, S.W. Pacific. J. Petrol. 14, 429–465. https://doi.org/10.1093/petrology/14.3.429.

Ewart, A., 1982. The mineralogy and petrology of Tertiary-Recent orogenic volcanic rocks with special reference to the andesitic–basaltic compositional range. In:

Thorpe, R.S. (Ed.), Andesites: Orogenic Andesites and Related Rocks. Wiley, Chichester, pp. 25–87.
Ewart, A., Collerson, K., Regelous, M., Wendt, J., Niu, Y., 1998. Geochemical evolution within the Tonga–Kermadec–Lau arc–back-arc systems: the role of varying mantle wedge composition in space and time. J. Petrol. 39, 331–368.
Fauria, K.E., Manga, M., 2018. Pyroclast cooling and saturation in water. J. Volcanol. Geotherm. Res. 362, 17–31.
Fauria, K.E., Manga, M., Wei, Z., 2017. Trapped bubbles keep pumice afloat and gas diffusion makes pumice sink. Earth Planet. Sci. Lett. 460, 50–59. https://doi.org/10.1016/j.epsl.2016.11.055.
Fiske, R.S., Cashman, K.V., Shibata, A., Watanabe, K., 1998. Tephra dispersal from Myojinsho, Japan, during its shallow submarine eruption of 1952-1953. Bull. Volcanol. 59, 262–275. https://doi.org/10.1007/s004450050190.
Garvin, J.B., Slayback, D.A., Ferrini, V., Frawley, J., Giguere, C., Asrar, G.R., Andersen, K., 2018. Monitoring and modeling the rapid evolution of Earth's newest volcanic island: Hunga Tonga Hunga Ha'apai (Tonga) using high spatial resolution satellite observations. Geophys. Res. Lett. 45, 3445–3452.
Global Volcanism Program, 2002. Smithsonian Institution, p. 1. https://doi.org/10.5479/si.GVP.BGVN200201-243091. Report on Unnamed (Tonga).
Global Volcanism Program, 2024. [Database] Volcanoes of the World (v. 5.2.1; 3 Jul 2024). Distributed by Smithsonian Institution, compiled by Venzke, E.. https://doi.org/10.5479/si.GVP.VOTW5-2024.5.2.
Global Volcanism Program, Smithsonian Institution, 2001. Report on Unnamed (Tonga). Bulletin of the Global Volcanism Network, p. 11. https://doi.org/10.5479/si.GVP.BGVN200111-243091.
Global Volcanism Program, Smithsonian Institution, 2003. Report on Unnamed (Tonga), 28. Bulletin of the Global Volcanism Network. https://doi.org/10.5479/si.GVP.BGVN200310-243091.
Global Volcanism Program, Smithsonian Institution, 2007. Report on Unnamed (Tonga), 32. Bulletin of the Global Volcanism Network. https://doi.org/10.5479/si.GVP.BGVN200705-243091.
Gupta, A.K., Bennartz, R., Fauria, K.E., Mittal, T., 2022. Eruption chronology of the December 2021 to January 2022 Hunga Tonga-Hunga Ha'apai eruption sequence. Communicat. Earth & Environ. 3, 314.
Hannington, M.D., Kopp, H., Schnabel, M., 2019. RV SONNE Fahrtbericht/Cruise Report SO267: ARCHIMEDES I: Arc Rifting, Metallogeny and Microplate Evolution–an Integrated Geodynamic, Magmatic and Hydrothermal Study of the Fonualei Rift System, NE Lau Basin, Suva (Fiji)–Suva (Fiji), 11.12. 2018–26.01. 201.
Henley, R.W., de Ronde, C.E., Arculus, R.J., Hughes, G., Pham, T.-S., Casas, A.S., Titov, V., Walker, S.L., 2024. The 15 January 2022 Hunga (Tonga) eruption: a gas-driven climactic explosion. J. Volcanol. Geotherm. Res. 451, 108077. https://doi.org/10.1016/j.jvolgeores.2024.108077.
Hoffmeister, J.E., Ladd, H.S., Alling, H.L., 1929. Falcon Island. Am. J. Sci. 18, 461–471.
Hutchinson, M.F., 1989. A new procedure for gridding elevation and stream line data with automatic removal of spurious pits. J. Hydrol. 106, 211–232. https://doi.org/10.1016/0022-1694(89)90073-5.
Jokiel, P.L., 1989. Rafting of reef corals and other organisms at Kwajalein Atoll. Mar. Biol. 101, 483–493. https://doi.org/10.1007/BF00541650.
Jokiel, P.L., Cox, E.F., 2003. Drift pumice at Christmas Island and Hawaii: evidence of oceanic dispersal patterns. Mar. Geol. 202, 121–133. https://doi.org/10.1016/S0025-3227(03)00288-3.
Jutzeler, M., Marsh, R., Carey, R.J., White, J.D.L., Talling, P.J., Karlstrom, L., 2014. On the fate of pumice rafts formed during the 2012 Havre submarine eruption. Nat. Commun. 5, 1–10. https://doi.org/10.1038/ncomms4660.
Jutzeler, M., Manga, M., White, J.D.L., Talling, P.J., Proussevitch, A.A., Watt, S.F.L., Cassidy, M., Taylor, R.N., Le Friant, A., Ishizuka, O., 2016. Submarine deposits from pumiceous pyroclastic density currents traveling over water: an outstanding example from offshore Montserrat (IODP 340). Geol. Soc. Am. Bull. https://doi.org/10.1130/B31448.1. B31448.1.
Jutzeler, M., Marsh, R., van Sebille, E., Mittal, T., Carey, R.J., Fauria, K.E., Manga, M., McPhie, J., 2020. Ongoing dispersal of the 7 August 2019 pumice raft from the Tonga arc in the southwestern Pacific Ocean. Geophys. Res. Lett. 47, e1701121.
Kano, K., Yamamoto, T., Ono, K., 1996. Subaqueous eruption and emplacement of the Shinjima Pumice, Shinjima (Moeshima) Island, Kagoshima Bay, SW Japan. J. Volcanol. Geotherm. Res. 71, 187–206.
Knafelc, J., Bryan, S.E., Jones, M.W., Gust, D., Mallmann, G., Cathey, H.E., Berry, A.J., Ferré, E.C., Howard, D.L., 2022. Havre 2012 pink pumice is evidence of a short-lived, deep-sea, magnetite nanolite-driven explosive eruption. Communicat. Earth & Environ. 3, 19.
Lacroix, A., 1939. Composition mineralogique et chimique des lavee des volcans des iles de l'ocean Pacifique situees entre l'Equateur et le tropique du Capricarne, le 175° de longitude ouest et le 165° de longitude est. Memor. de l'Academ. des Sci. Paris 63, 1–97.
Lacroix, A., 1940. Les charateristiques des laves situées au sud de l'equateur, formant la limite du domaine circumpacifique dans la région des Nouvelle-Hebrides et de la fosse Tonga-Kermadec. Acadam. Sci. Paris 211, 37–40.
Le Mével, H., Miller, C.A., Ribó, M., Cronin, S., Kula, T., 2023. The magmatic system under Hunga volcano before and after the 15 January 2022 eruption. Sci. Adv. 9 p. eadh3156.
Lynett, P., McCann, M., Zhou, Z., Renteria, W., Borrero, J., Greer, D., Fa'anunu, O., Bosserelle, C., Jaffe, B., La Selle, S., 2022. Diverse tsunamigenesis triggered by the Hunga Tonga-Hunga Ha'apai eruption. Nature 609, 728–733.
Manga, M., Mitchell, S.J., Degruyter, W., Carey, R.J., 2018. Transition of eruptive style: Pumice raft to dome-forming eruption at the Havre submarine volcano, Southwest Pacific Ocean. Geology 46, 1075–1078.
Manga, M., et al., 2018a. The pumice raft-forming 2012 Havre submarine eruption was effusive. Earth Planet. Sci. Lett. 489, 49–58. https://doi.org/10.1016/j.epsl.2018.02.025.
Melson, W.G., Jarosewich, E., Lundquist, C.A., 1970. Volcanic Eruption at Metis Shoal, Tonga, 1967-1968: Description and Petrology. Smithson. Contrib. Earth Sci. 1–18. https://doi.org/10.5479/si.00810274.4.1.
Mitchell, S.J., McIntosh, I.M., Houghton, B.F., Carey, R.J., Shea, T., 2018. Dynamics of a powerful deep submarine eruption recorded in H2O contents and speciation in rhyolitic glass: the 2012 Havre eruption. Earth Planet. Sci. Lett. 494, 135–147. https://doi.org/10.1016/j.epsl.2018.04.053.
Mitchell, S.J., Fauria, K.E., Houghton, B.F., Carey, R.J., 2021. Sink or float: microtextural controls on the fate of pumice deposition during the 2012 submarine Havre eruption. Bull. Volcanol. 83, 80. https://doi.org/10.1007/s00445-021-01497-6.
NASA. https://worldview.earthdata.nasa.gov/?v=-175.42198623135474,-9.021735394030717,-173.66686787395471,-17.828196260427024&t=2019-08-08- T04%3A50%3A46Z, 2019.
Newhall, C.G., Self, S., 1982. The volcanic explosivity index (VEI) an estimate of explosive magnitude for historical volcanism. J. Geophys. Res. Oceans 87, 1231–1238. https://doi.org/10.1029/JC087iC02p01231.
Ohno, Y., Iguchi, A., Ijima, M., Yasumoto, K., Suzuki, A., 2022. Coastal ecological impacts from pumice rafts. Sci. Rep. 12, 11187.
Oikawa, T., 2021. Fukutoku Okanoba eruption in Ogasawara Islands, Japan: Abstract Vol. Annu. Meet. Volcanol. Soc. Jpn, 2021, pp. 1–34.
Pope, E.L., Jutzeler, M., Cartigny, M.J., Shreeve, J., Talling, P.J., Wright, I.C., Wysoczanski, R.J., 2018. Origin of spectacular fields of submarine sediment waves around volcanic islands. Earth Planet. Sci. Lett. 493, 12–24.
Preine, J., et al., 2024. Hazardous explosive eruptions of a recharging multi-cyclic island arc caldera. Nat. Geosci. 17, 323–331. https://doi.org/10.1038/s41561-024-01392-7.
Putirka, K.D., 2008. Thermometers and barometers for volcanic systems. Rev. Mineral. Geochem. 69, 61–120.
Reagan, M., Turner, S., Handley, H., Turner, M., Beier, C., Caulfield, J., Peate, D., 2017. 210 Pb-226 Ra disequilibria in young gas-laden magmas. Sci. Rep. 7, 1–12.
Roman, L., Bryan, S., Bool, N., Gustafson, L., Townsend, K., 2021. Desperate times call for desperate measures: non-food ingestion by starving seabirds. Mar. Ecol. Prog. Ser. 662, 157–168.
Ryan, W.B.F., et al., 2009. Global Multi-Resolution Topography synthesis. Geochem. Geophys. Geosyst. 10 https://doi.org/10.1029/2008GC002332.
Sail Surf, R.O.A.M., 2019. Report of Volcanic Rubble Slick dangerous to Vessels. https://www.facebook.com/sailsurfroam/posts/3045949342087617:0.
Sano, T., Tani, K., Murch, A.P., 2020. Major and trace element analyses of igneous rocks and sediments by X-ray fluorescence spectrometry using glass bead and pressed powder pellet. Bull. Natl. Mus. Nat. Sci. Ser. C 46, 1–14.
Seabrook, S., Mackay, K., Watson, S., Clare, M., Hunt, J., Yeo, I., Lane, E., Clark, M., Wysoczanski, R., Rowden, A., 2023. Pyroclastic Density Currents Explain Far-Reaching and Diverse Seafloor Impacts of the 2022 Hunga Tonga Hunga Ha'apai Eruption.
Simkin, T., Fiske, R.S., 1984. Krakatau 1883: The Volcanic Eruption and its Effects: Washington. Smithsonian Institution Press, D.C., p. 464
Tanakadate, H., 1935. Evolution of a new volcanic islet near Io-zima (Satsuma Prov.). In: Proceedings of the Imperial Academy, 11, pp. 152–154.
Turner, S., Hawkesworth, C., 1997. Constraints on flux rates and mantle dynamics beneath island arcs from Tonga-Kermadec lava geochemistry. Nature 389, 568–573. https://doi.org/10.1038/39257.
Turner, S., Caulfield, J., Rushmer, T., Turner, M., Cronin, S., Smith, I., Handley, H., 2012. Magma evolution in the primitive, intra-oceanic Tonga arc: Rapid petrogenesis of dacites at Fonualei volcano. J. Petrol. 53, 1231–1253.
Vaughan, R.G., Webley, P.W., 2010. Satellite observations of a surtseyan eruption: Hunga Ha'apai, Tonga. J. Volcanol. Geotherm. Res. 198, 177–186.
Vázquez-Prada, G., Jaramillo, E., Morales, G., Silva, R., 2013. First record of Lepas spp. (Cirripedia: Thoracica: Lepadiformes) attached to pumice from the Cordón-Caulle eruption along the central-south Chilean coast. Marine Biodiversit. Records 6.
Velasquez, E., Bryan, S.E., Ekins, M., Cook, A.G., Hurrey, L., Firn, J., 2018. Age and area predict patterns of species richness in pumice rafts contingent on oceanic climatic zone encountered. Ecol. Evol. 8, 5034–5046.
von Lichtan, I.J., White, J.D.L., Manville, V., Ohneiser, C., 2016. Giant rafted pumice blocks from the most recent eruption of Taupo volcano, New Zealand: Insights from palaeomagnetic and textural data. Journal of Volcanology and Geothermal Research ISSN 318, 73–88. https://doi.org/10.1016/j.jvolgeores.2016.04.003. https://www.sciencedirect.com/science/article/pii/S037702731630035X.
Yeo, I.A., Dobson, K., Josso, P., Pearce, R.B., Howarth, S.A., Lusty, P.A.J., Le Bas, T.P., Murton, B.J., 2018. Assessment of the mineral resource potential of Atlantic ferromanganese crusts based on their growth history, microstructure, and texture. Minerals 8. https://doi.org/10.3390/min8080327.
Yeo, I.A., McIntosh, I.M., Bryan, S.E., Tani, K., Dunbabin, M., Metz, D., Collins, P.C., Stone, K., Manu, M.S., 2022. The 2019–2020 Volcanic Eruption of Late'iki (Metis Shoal), vol. v. 12. Scientific Reports, Tonga, p. 7468. https://doi.org/10.1038/s41598-022-11133-8.
Yoshida, K., Tamura, Y., Sato, T., Hanyu, T., Usui, Y., Chang, Q., Ono, S., 2022. Variety of the Drift Pumice Clasts from the 2021 Fukutoku-Oka-no-Ba Eruption, vol. v. 31. Island Arc, Japan, p. e12441.